

INFLUENCE BY CALCAREOUS DEPOSITS ON FATIGUE
CRACK CLOSURE IN STEEL

BY

Ai-Kuo Lee

A Thesis Submitted to the Faculty of the
College of Engineering
in Partial Fulfillment of the Requirements for the Degree
of
Master of Science in Engineering

Florida Atlantic University

Boca Raton, Florida

August 1986

INFLUENCE BY CALCAREOUS DEPOSITS ON FATIGUE

CRACK CLOSURE IN STEEL

BY

Ai-Kuo Lee

This thesis was prepared under the direction of the candidate's advisor, Dr. William H. Hartt, Department of Ocean Engineering. It was submitted to the faculty of the College of Engineering and was accepted in partial fulfillment of the requirements for the degree of Master of Science in Engineering.

SUPERVISORY COMMITTEE



Thesis Advisor



Chairman, Department of
Ocean Engineering



Dean, College of Engineering



Dean for Advanced Studies

Date

June 30, 1986

ACKNOWLEDGEMENT

I wish to express my most sincere thanks to Dr. William H. Hartt, Professor of Ocean Engineering, for his unceasing patience and excellent guidance in preparation of this thesis.

The thanks are also extended to Dr. D. V. Reddy, Professor of Ocean Engineering, and Dr. Samuel Smith, Assistant Professor of Ocean Engineering, for their suggestions and to Mr. Shirish S. Rajpathak, Mr. Ravi M. Krishnamurtny, Mr. Anil K. Sablok and Mr. Tien-Jen Wang, for their dedication to the project and their friendship.

Lastly, and of course most important, I wish to pay tribute to my beloved parents and wife.

ABSTRACT

Author: Ai-Kuo Lee
Title: Influence by Calcareous Deposits on
Fatigue Crack Closure in Steel
Institution: Florida Atlantic University
Degree: Master of Science in Engineeringg
Year: 1986

A model for calcareous deposit induced fatigue crack closure has been previously reported based upon the criterion that the deposit thickness within the crack equals or exceeds one-half the minimum crack opening displacement. In the present paper an expanded and refined model is proposed by considering (1) compaction of calcareous deposits during the closure period of the stress cycle and (2) the relationship between R ratio and threshold stress intensity range. Compression tests upon calcareous films grown on steel surfaces have been performed, and these reveal the change in deposit thickness as a function of stress. The implications of these models to calcareous deposit induced fatigue crack closure are discussed in terms of mechanical and electrochemical parameters.

TABLE OF CONTENTS

LIST OF TABLES	vi
LIST OF FIGURES	vii
I. INTRODUCTION	1
1.1 Calcareous Deposits	1
1.2 Corrosion Fatigue	6
1.3 Crack Closure	17
1.4 Purpose of Thesis	20
II. MODEL DEVELOPMENT	24
III. EXPERIMENTAL PROCEDURE	30
3.1 Specimens	30
3.2 Equipment Description	33
3.3 Procedure	33
IV. RESULT AND DISCUSSION	36
4.1 Calcareous Deposit Thickness	36
4.2 Wedging Stress Analysis	43
4.3 The Limit of Corrosion Fatigue Crack Closure	49
V. CONCLUSIONS	57
BIBLIOGRAPHY	59

LIST OF TABLES

Table 3-1	Exposure Time for Different Specimens	32
Table 4-1	Reduction Percentage of Calcareous Deposition Thickness	39

LIST OF FIGURES

Figure		Page
1-1	Cathodic protection by superposition of impressed current on local-action current ...	2
1-2	Polarization diagram illustrating principle of cathodic protection	2
1-3	Schematic illustration of the pH profile in the electrolyte adjacent to a cathodically polarized metal surface	4
1-4	Corrosion fatigue of steel cable	8
1-5	Fatigue crack propagation for various FCC, BCC, and HCP metals, data verify power relationship between ΔK and da/dN	11
1-6	Corrosion-Fatigue-Crack growth rates for API X-70 steel in 3.5 percent NaCl solution	12
1-7	Corrosion-Fatigue-Crack growth rate for specimens at an electrochemical potential of $-1.10V$ Ag/AgCl	14
1-8	Corrosion-Fatigue-Crack growth rates in 3.5 percent NaCl solution at zinc potential, $R=0.4$ and three frequencies	16
1-9	Crack surface interference results in crack opening K_{op} to be above zero, ΔK_{eff} defined as $K_{max} - K_{op}$	19
1-10	Schematic illustration of possible mechanisms of fatigue crack closure at near-threshold stress intensities	21
2-1	Schematic representation of fatigue crack ...	26
3-1	Specimen	31
3-2	Experimental setup	34

4-1	Photograph of calcareous deposits after compression	37
4-2	Photograph of calcareous deposits before and after compression (#06, -0.85V SCE)	38
4-3	Thickness of deposits vs. exposure time (-0.85V SCE)	40
4-4	Thickness of deposits vs. exposure time (-1.00V SCE)	41
4-5	Applied loads vs. the reduction of thickness (#10)	44
4-6	Applied loads vs. the reduction of thickness (#29)	45
4-7	Applied loads vs. the reduction of thickness (#06)	46
4-8	Applied loads vs: the reduction of thickness (#18)	47
4-9	Plot of limit crack growth rate vs. time	50
4-10	Plot of limit fatigue crack growth rate vs.R	52
4-11	Plot of limit (da/dt) vs. R for different frequency	54
4-12	Plot of limit (da/dN) vs. R for different frequency	55

I. INTRODUCTION

1.1 Calcareous Deposits

Cathodic protection is an important method of corrosion prevention. It is also effective in reducing or eliminating corrosion fatigue. The basic concept of cathodic protection is to prevent ions of a corroding metal from entering the electrolyte. Figure 1-1 illustrates that current leaves the auxiliary anode and enters both the cathodic and anodic areas of the corroding metal. The cathodic areas are polarized by an external current to the open-circuit potential for the anodic reaction. Local action current is eliminated as the anodic areas also must be at this potential (assuming that IR drop is negligible) and the entire metal surface is maintained at the same potential. Consequently, corrosion does not occur so long as the required external current is maintained.

The corresponding polarization diagram is given in Fig.1-2. If the potential is shifted from ϕ_{corr} to 'a' by

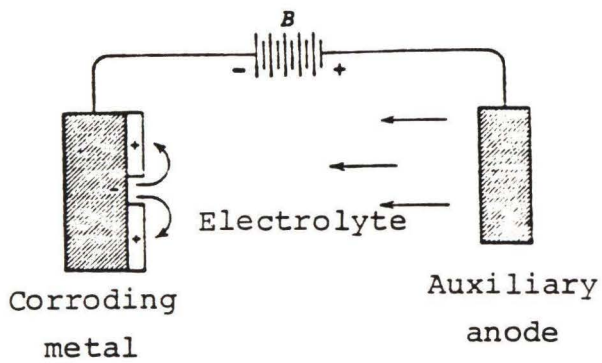


Figure 1-1. Cathodic protection by superposition of impressed current on local-action current.

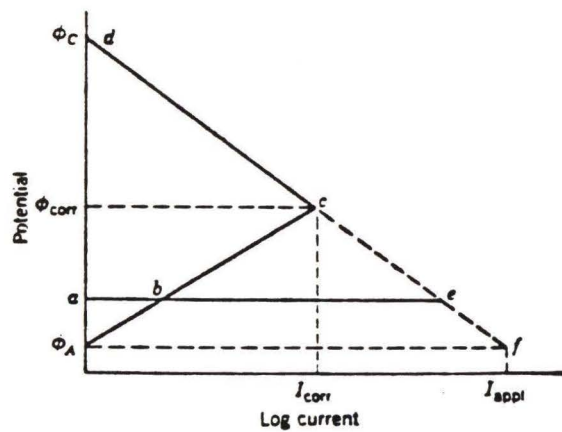


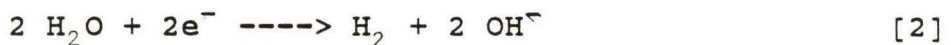
Figure 1-2. Polarization diagram illustrating principle of cathodic protection.

applied current 'b-e', the corrosion current decreases from I_{corr} to a-b. Moving from 'e' to 'f', corresponding to ϕ_A , the open-circuit potential corrosion current 'a-b' become zero and applied current for complete cathodic protection equals I_{applied} (1).

For most cathodic surfaces in aerated waters, the principal reaction is



In case where potential is more negative than the reversible hydrogen electrode, a second reaction



also occurs. In either case, the production of hydroxyl ions results in an increase in pH for the electrolyte adjacent to the metal surface. This situation is presented schematically in Fig. 1-3. In sea water pH is controlled by the carbon dioxide system, as expressed by the following reactions:

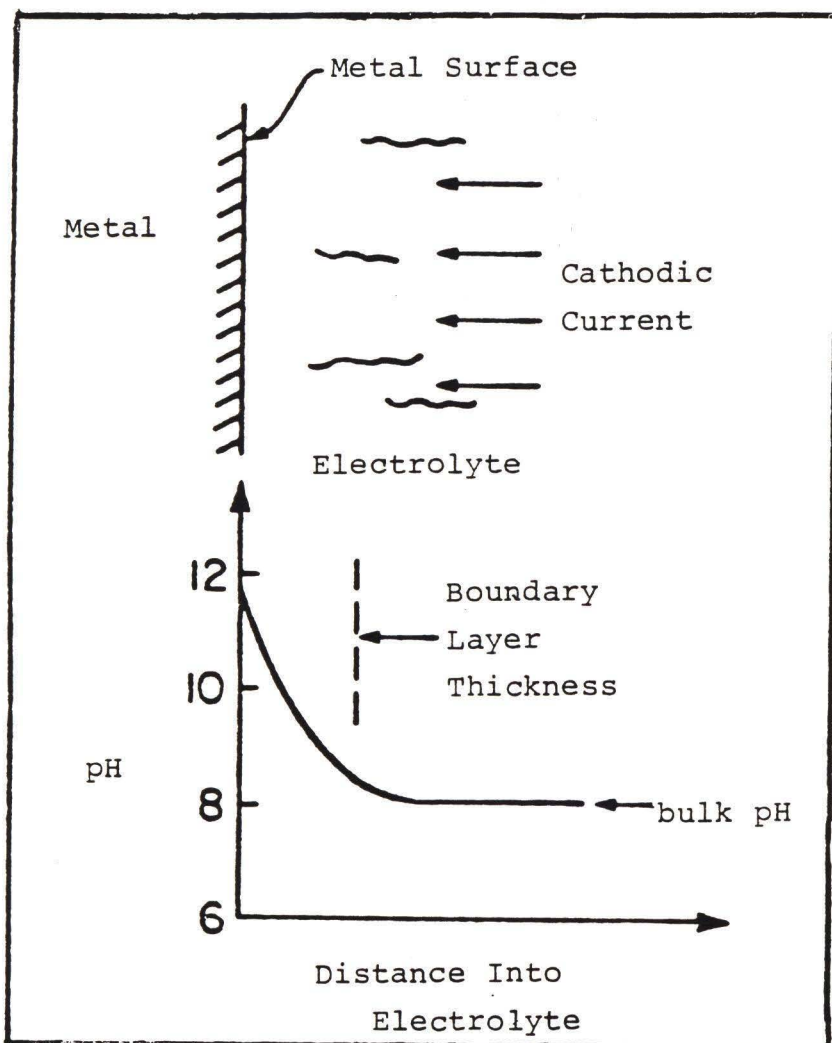
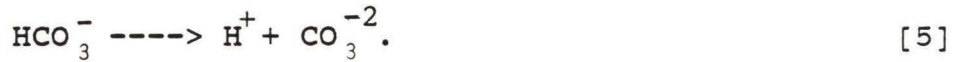
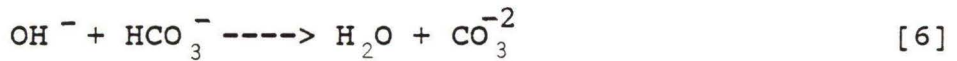


Figure 1-3. Schematic illustration of the pH profile in the electrolyte adjacent to a cathodically polarized metal surface.



If OH^- is added to the system as a consequence of one of the above cathodic processes, then the reactions



are expected (2).

Calcareous deposits are not comprised solely of calcium carbonate. There are also other components; for example, MgCO_3 and SrCO_3 (3). Deposit chemistry may be complex and variable depending upon the condition of formation, but the material is comprised primarily of CaCO_3 and $\text{Mg}(\text{OH})_2$. The situation may be made even more complex by the fact that nucleation and growth rates of

calcareous deposits are dependent upon potential, time, pressure, temperature, sea water chemistry, velocity, and substrate surface condition (2).

Recent anomalous departures (4-7) from the general fatigue crack growth rate trend in natural or synthetic sea water have been observed, when specimens were cathodically protected. These observations included both a reduction in fatigue crack growth rate and a complete arrest. Velden et al (8) concluded that the mechanism responsible for crack growth retardation of structural steel in sea water was due to corrosion product wedging, which increased the minimum K and, hence, reduced the stress intensity range ΔK . The influence of corrosion product wedging depends on the amount of crack closure, which increases at lower R values. In this paper, calcareous deposits are thought to have a wedging effect on the crack, causing reduction in effective stress intensity range and inducing crack closure.

1.2 Corrosion Fatigue

Corrosion fatigue behavior is a type of failure caused by fluctuating load in the presence of a particular

environment. Gilbert (9) listed some characteristics of corrosion fatigue behavior. Most notable for ferrous alloys was the loss of the endurance limit under corrosion fatigue conditions, and he emphasized the necessity of specifying the number of cycles when referring to any corrosion fatigue limit. In Figure 1-4, LaQue (10) illustrated the cyclic stress-endurance (S-N) diagram for a steel cable under three different test conditions. When the cable was fatigued in air at a stress below the fatigue or endurance limit, failure did not occur. However, when this cable was tested in sea water, the fatigue limit did not exist; and fatigue life was reduced due to the conjoint actions of stress and corrosion.

In addition Gillbert (9) noted that:

(1) Corrosion fatigue in immersed conditions is an electrochemical phenomenon, as shown by the fact that it can sometimes be prevented by cathodic protection or by adding suitable inhibitors to the corroding solution.

(2) Corrosion fatigue cracks are usually transcrystalline, though in a minority of cases they may be intercrystalline.

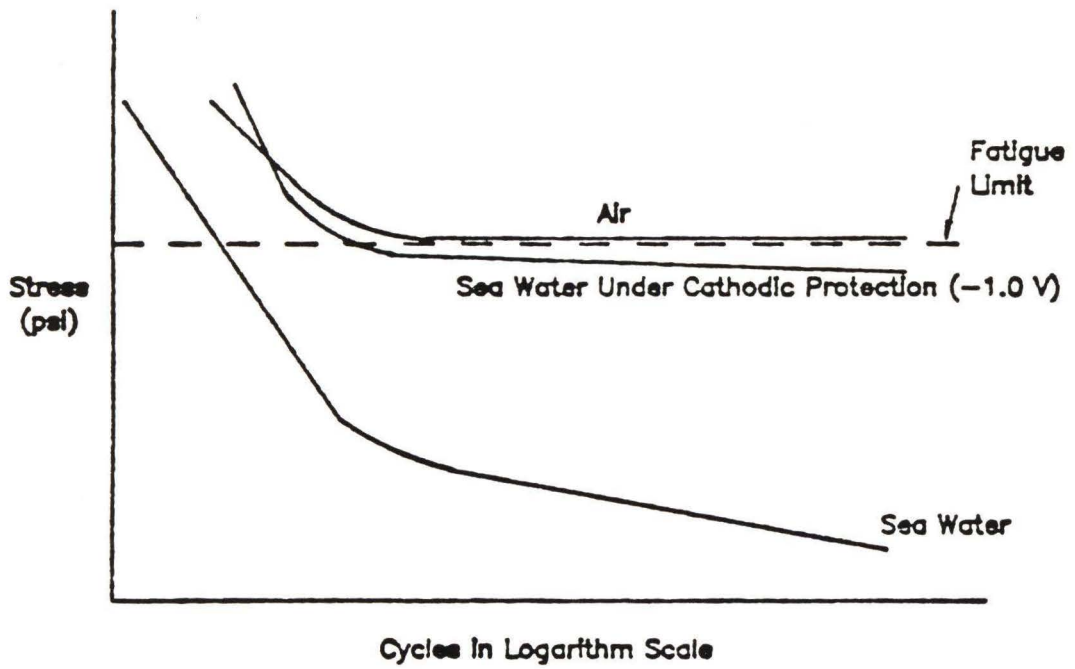


Figure 1-4. Corrosion Fatigue of Steel Cable

(3) Corrosion fatigue usually produces a large number of cracks (as distinct from ordinary fatigue). Consequently, the face of the fracture frequently shows a characteristic serrated appearance, and many subsidiary cracks can usually be found near the main one.

(4) Corrosion fatigue limits for steels are often relatively insensitive to changes in metallurgical conditions, such as those produced by cold working, heat treatment, etc..

Influential variables to corrosion fatigue may be listed in three categories: (1) mechanical (stress or stress intensity, stress ratio, loading frequency, specimen geometry, constant or variable amplitude loading, etc.), (2) metallurgical (alloy composition, microstructure, strength, etc.), and (3) environmental variable (temperature, electrolyte composition, pH, potential, coating, etc.) (11). Based upon Gillbert's conclusion (see (4) above), however, metallurgical variables can be ignored.

EFFECT OF STRESS INTENSITY FACTOR RANGE

Paris (12) postulated that the stress intensity factor - itself a function of stress and crack length - was the overall controlling factor in the fatigue crack growth rate (FCGR) process. By plotting da/dN versus ΔK , a correlation was observed for different materials as shown in Fig.1-5, which suggested a relationship of the form

$$da/dN = c \Delta K^m \quad [8]$$

where da/dN = fatigue crack growth rate

ΔK = stress intensity factor range ($\Delta K = K_{max} - K_{min}$)

$c, m = f(\text{material variable, environment, frequency, temperature, stress ratio etc.})$

EFFECT OF STRESS RATIO

Vosikovsky (13) conducted tests at three positive R values and his results are given in Figure 1-6. The ΔK vs. da/dN curves were shifted upward (increased da/dN) as R value increased. The environmental effects were most pronounced at intermediate ΔK levels. Overprotection to

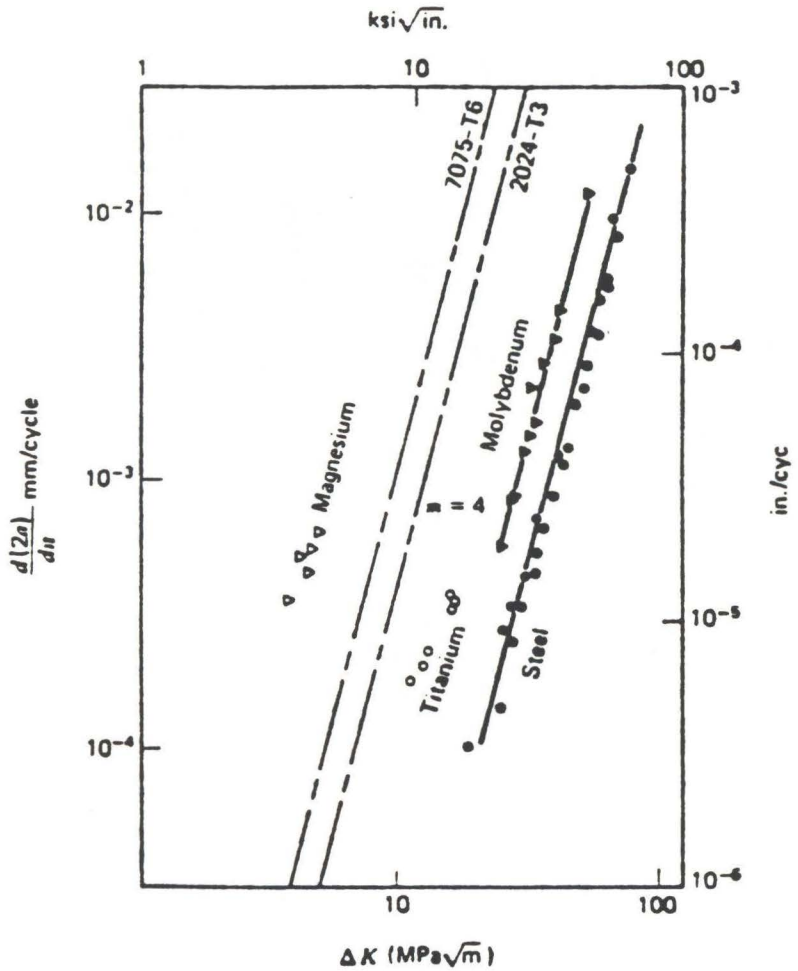


Figure 1-5. Fatigue crack propagation for various FCC, BCC, and HCP metals, Data verify power relationship between ΔK and da/dN .

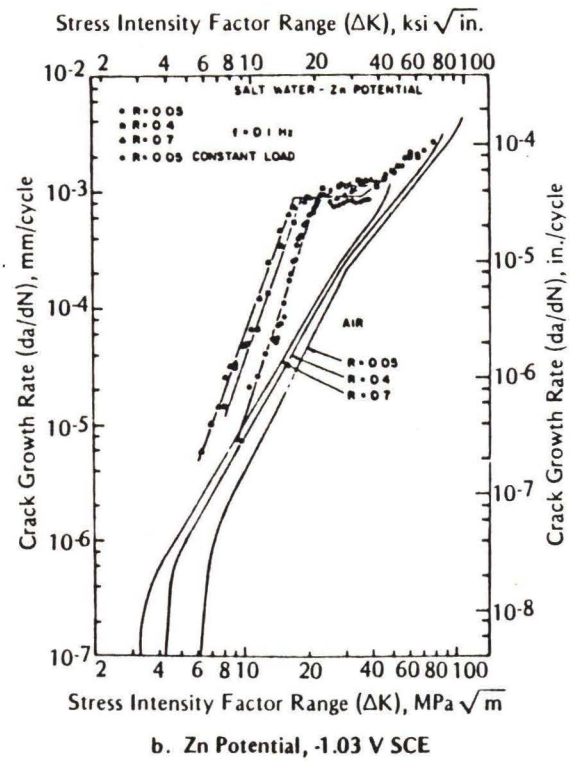
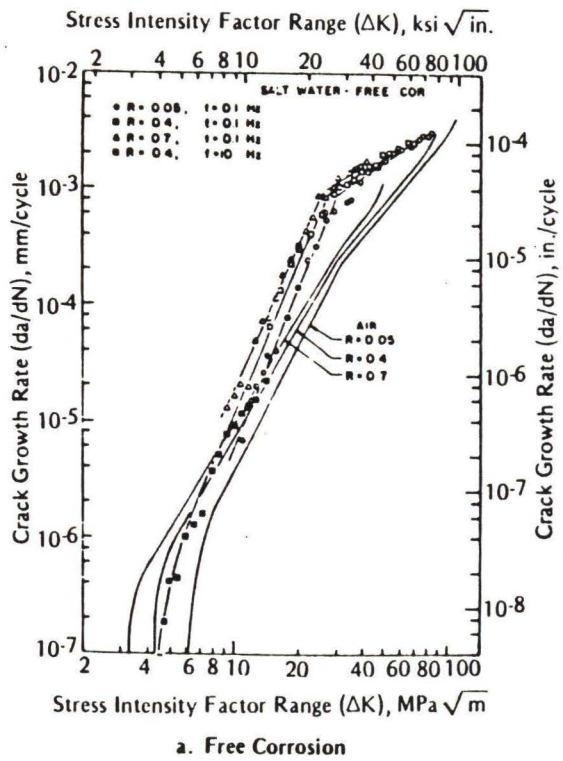


Figure 1-6. Corrosion-Fatigue-Crack Growth Rates for API X-70 Steel in 3.5 Percent NaCl Solution

-1.03 V (vs. SCE) was detrimental because it produced localized hydrogen embrittlement near the crack tip. Scott and Silvester (14) conducted experiments in seawater at 5 to 10 C and at -1.10V Ag/AgCl; their results are presented in Figure 1-7. The crack growth rates were accelerated by the seawater environment and by increasing stress ratio. There is an upper bound curve for all of the data except intermediate ΔK level with cathodic protection, where sharp bumps in the ΔK vs. da/dN curves, similar to those reported by Vosikovsky, were found. At low ΔK level some points are labelled as experimental artifacts because calcareous deposits formed in the crack tip and decreased the effective local stress intensity; hence, the da/dN value decreased. When R ratio was increased on the same specimen, crack growth rate was initially higher, which is also indicative of an artifact. Barson (15) suggested a relation between fatigue-crack-propagation threshold of steels and load ratio for $R > 0.1$ as

$$\Delta K_{th} = 6.4 (1 - 0.85R).$$

[9]

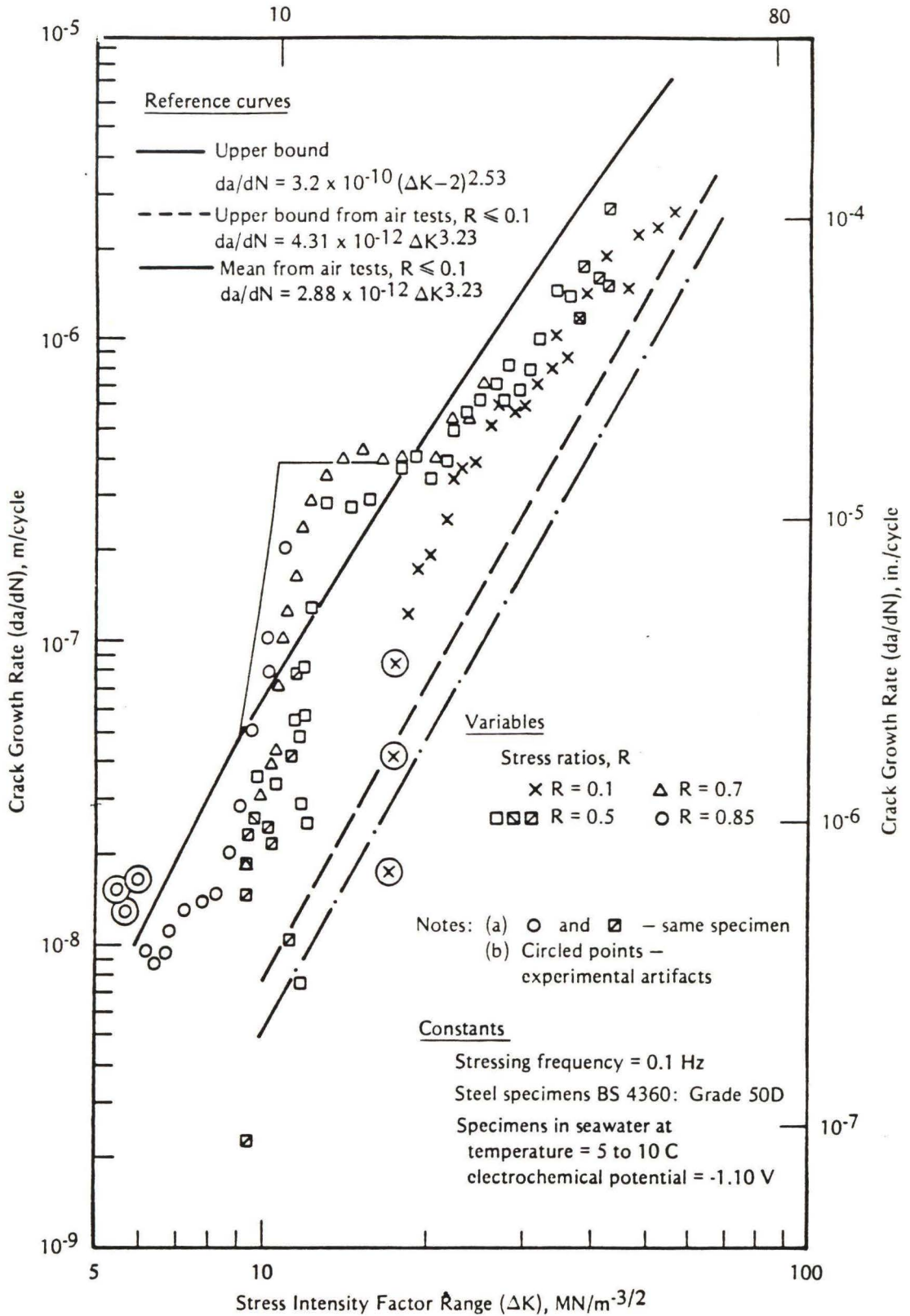


Figure 1-7. Corrosion-Fatigue-Crack Growth Rate for Specimens at an Electrochemical Potential of -1.10V Ag/AgCl

EFFECT OF CYCLIC FREQUENCY

It is generally observed that lower frequencies cause increased da/dN values at intermediate ΔK levels. Vosikovsky (13,16) found similar frequency effects for both API X-65 and X-70 steels tested in 3.5 percent NaCl solution (Figure 1-8). At reduced frequencies, the kink in the curves for overprotection conditions (Zn potential, -1.03V SCE) was shifted to higher da/dN values and ΔK levels. Scott and Silvester (17) found that decreasing the frequency from 10 to 1 Hz had little effect on crack growth rate but that decreasing it to 0.1 and 0.05 Hz resulted in crack growth rates about four to five times those in air, when ΔK was about 20.0 Mpa \sqrt{m} at $R = 0.1$, and in seawater at 68 ° F.

EFFECT OF ENVIRONMENT VARIABLES

Effects of variations in water temperature from 30 to 75° F (-1 to 24° C) were evaluated in a combination of two investigations (17,18). Socie and Antolovich (18) determined that crack-growth rate increased by about a factor of two as temperature increased from 30 to 39 ° F(-1

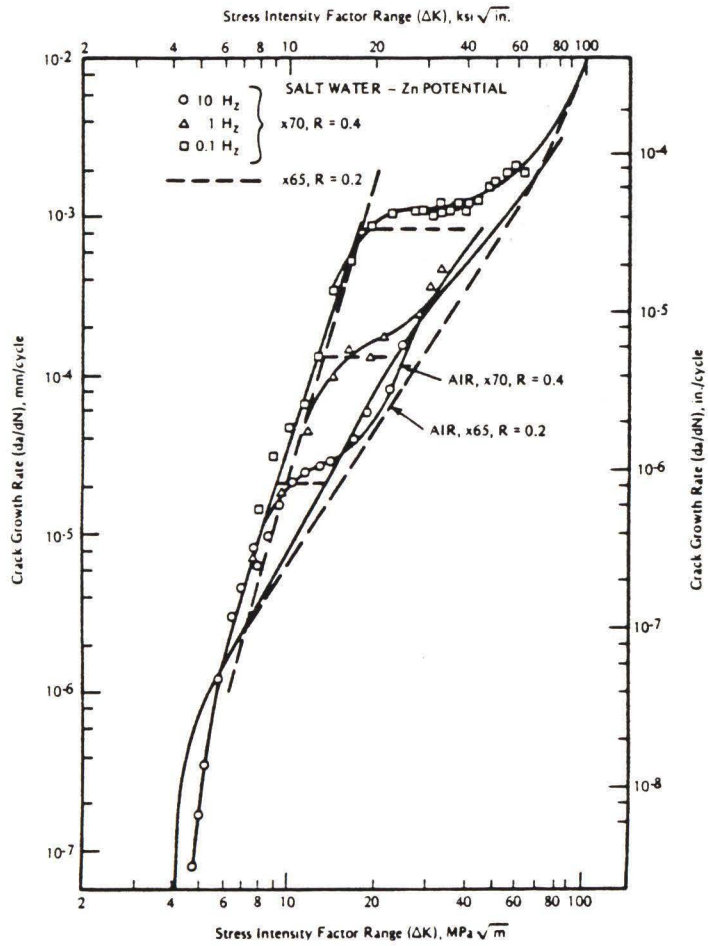


Figure 1-8. Corrosion-Fatigue-Crack Growth Rates in 3.5 Percent NaCl Solution at Zinc Potential, $R = 0.4$, and Three Frequencies.

to 4°C) up to 68 to 75°F (20 to 24°C) in the intermediate ΔK regime. At low ΔK levels, the results of Scott and Silvester (17) showed that increasing temperature from 41 to 68°F (5 to 20°C) had little effect.

Oxygen levels of 1 mg/l and 7 to 8 mg/l (air saturation) were investigated by Scott and Silvester (17). The reduction in oxygen level significantly decreased crack growth rates under free-corrosion conditions, but had no significant influence under cathodic protection at -0.8 V Ag/AgCl and -1.0 V Ag/AgCl.

1.3 Crack Closure

The concept of fatigue crack closure was first put forth by Elber (19). He noted that a fatigue crack tip remained closed over a significant portion of the loading cycle. There are many factors that can influence corrosion fatigue crack closure. However, the range of the stress intensity factor, ΔK , has been shown to be a major controlling parameter for crack closure.

Elber (19) suggested that residual tensile displacements, resulting from the plastic damage of fatigue crack extension, may interfere along the crack surface in the wake of an advancing crack front and cause the crack to close at a stress above the minimum applied level. This hypothesis was verified by compliance measurements taken from fatigued test panels, which showed that an effective change in crack length (i.e. change in compliance) occurred prior to any actual change in crack length. In other words, the crack was partially closed for a portion of the loading cycle and did not open fully until a certain opening K level, K_{op} , was applied. As a result, the damaging portion of the cyclic load excursion would be restricted to that part of the load cycle which acted on a fully opened crack. From Figure 1-9, the effective stress intensity factor range, ΔK_{eff} , would be denoted by the opening level K_{op} and K_{max} , rather than by the applied ΔK level $K_{max} - K_{min}$.

Ritchie (20) considered crack closure during corrosion fatigue. When near-threshold crack growth occurs at low load ratios in moist environments, corrosion products of a thickness comparable with the size of crack tip opening

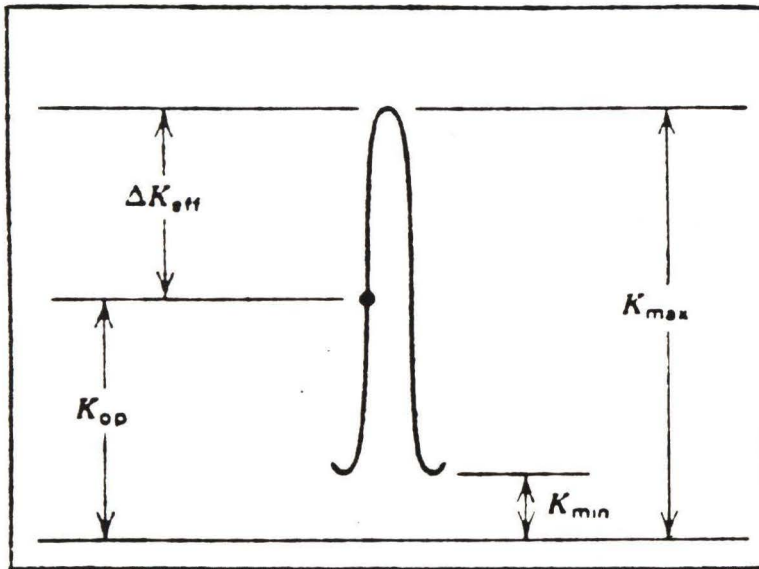


Figure 1-9. Crack Surface interference results in crack opening K_{op} to be above zero. ΔK_{eff} defined as $K_{max} - K_{op}$.

displacements can build up near the crack tip, thus providing a mechanism for enhanced closure such that the crack is wedged-opened at opening stress intensities, which is defined as Figure 1-10. Scott et al (21) suggested that crack retardation at low values of crack tip stress intensity range, ΔK , had long been suspected as being caused by the deposition of calcareous cathodic reaction products from seawater. These precipitates (which cannot form from NaCl solution) had been observed to cause the minimum value of the measured crack opening displacement to increase while the maximum value remained virtually unchanged over the same time span, thus wedging the crack open. This crack plugging mechanism is primarily responsible for the closure of corrosion fatigue crack growth in steel cathodically protected in seawater.

1.4 Purpose of Thesis

The focus of this research program has been to compare experimentally measured deposit growth kinetics data with an expression for crack opening displacement and to establish the conditions for which crack closure should and should not occur. In 1985, Mao(22) assumed that fatigue

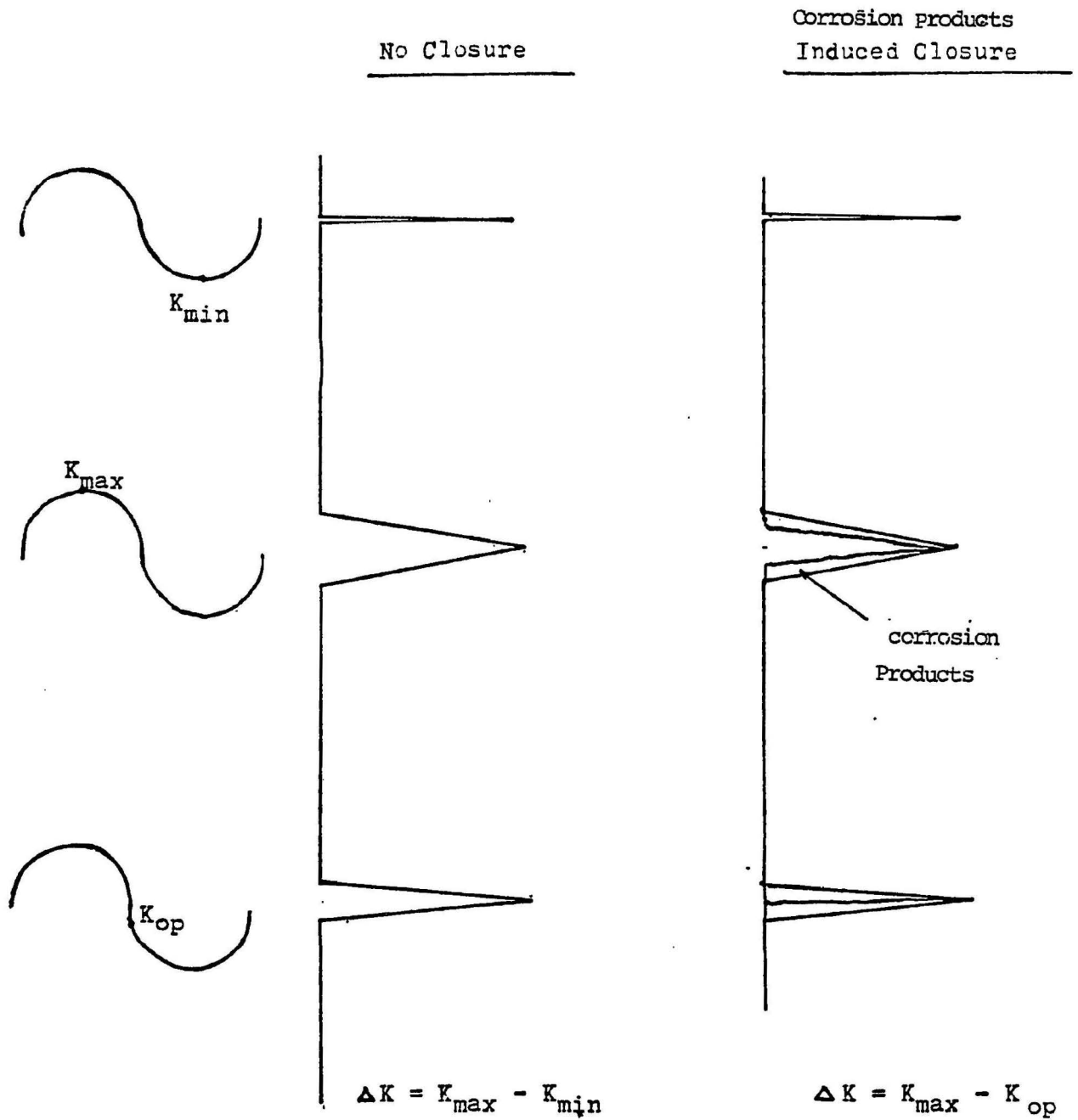


Figure 1-10. Schematic illustration of possible mechanisms of fatigue crack closure at near-threshold stress intensities.

crack closure occurs when the deposit thickness within the crack equals or exceeds one-half the minimum crack opening displacement. There are several additional assumptions he made such as:

(1) deposit thickening rate within an occluded cell is the same as upon a boldly exposed surface.

(2) crack growth rate with time, da/dt , is constant.

Mao's (21) conclusions were as follow:

(1) Fatigue crack closure may occur over a greater range of crack growth rate for lower R values.

(2) The minimum condition of closure for the potential $-0.85V$ occurs at a lesser crack growth rate than for the potential $-1.00V$.

However, his assumptions did not take into account that the deposits are porous and that the contact may result in compaction and reduction in deposit thickness and didnot consider that load ratio is a possible variation of threshold stress intensity range.

As an extention of Mao's model, additional factors were considered in this rēsearch for example: (1) thickness of calcareous deposits when compressed, (2) the

reduction in the range of the stress intensity, ΔK , which is an important controlling parameter for fatigue crack growth rate, (3) the influence of fatigue frequency, and (4) the variation of threshold stress intensity range with load ratio.

II. MODEL DEVELOPMENT

In this research a simulation model of depressed calcareous deposit induced fatigue crack closure is presented. From Mao's(22) assumption, when the thickness of calcareous deposit, y , equals the minimum half-crack opening on each cycle, v_{\min} , fatigue crack closure should occur. For this situation

$$y = v_{\min} \cdot \quad [10]$$

Calcareous deposits will be formed in a simulated fatigue crack specimen to quiescent natural sea water under conditions of cathodic polarization. Deposit thickness which is function of time, potential, temperature etc. can be measured by scanning electron microscopy (23).

The classical equation (24) for crack opening displacement is

$$v_{\min} = \frac{\sigma_{\min}^2}{E} [a^2 - x^2]^{1/2} \quad [11]$$

where E is Young's modulus, σ_{\min} is applied minimum stress, a is crack length, and x is position along the crack, as defined in Figure 2-1.

The relation between fatigue crack growth rate da/dN , and stress intensity range, ΔK , may be represented as (25)

$$da/dN = c [\Delta K - \Delta K_{th}]^m \quad [12]$$

where c and m are constants ($3.2 \cdot 10^{-10}$ and 2.53, respectively for crack growth rate in m/cycle and ΔK in Mpa \sqrt{m}).

From fundamental principles, the stress intensity is expressed by

$$K = \sigma (\pi a)^{1/2} \quad [13]$$

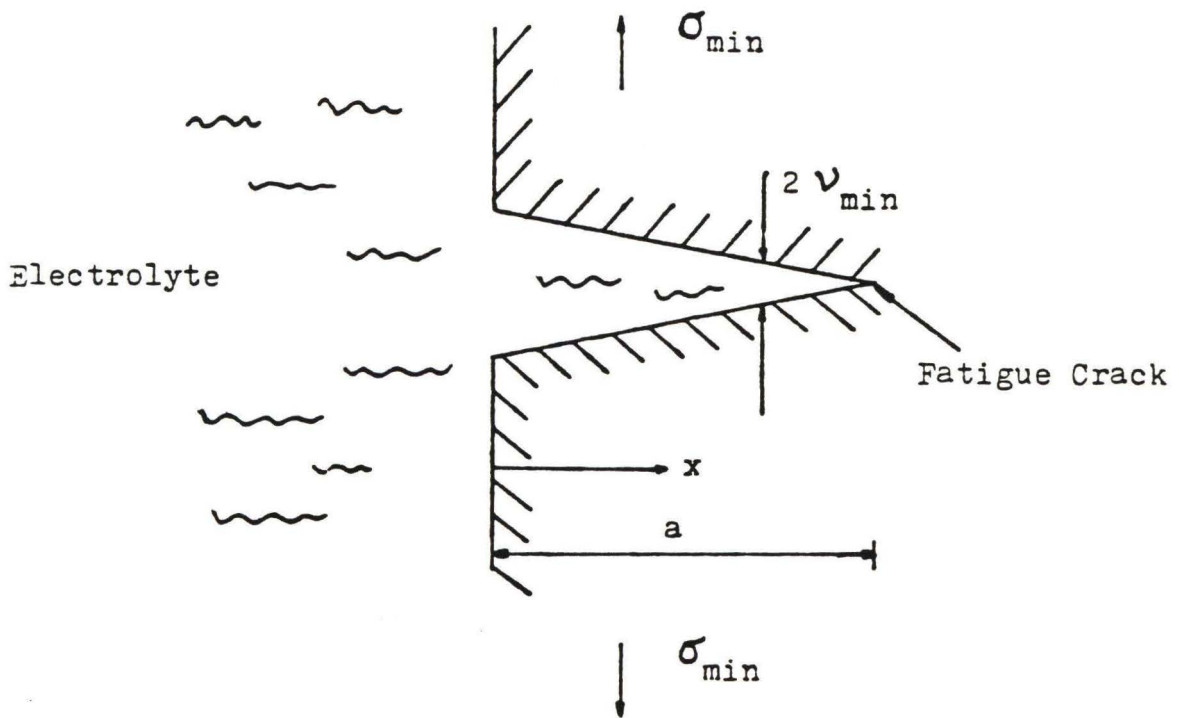


Figure 2-1. Schematic representation of fatigue crack.

where stress intensity range is

$$\Delta K = K_{\max} - K_{\min}. \quad [14]$$

The interrelation of fatigue crack propagation threshold range, ΔK_{th} , and stress ratio, $R = K_{\min} / K_{\max}$, has been proposed by Barson (15) as

$$\Delta K_{th} = 6.4 (1 - 0.85R), \quad R > 0.1. \quad [15]$$

Substituting equations of [14] and [15] into equation [12] yields

$$da/dN = c[K_{\max} - K_{\min} - 6.4(1 - 0.85R)]^m, \quad R > 0.1 \quad [16]$$

From equation [11],

$$K_{\max} = \frac{K_{\min}}{R} = \frac{\sigma_{\min} (\pi a)^{1/2}}{R} = \frac{\nu_{\min} E}{2R(a - x)^{1/2}} (\pi a)^{1/2} \quad [17]$$

$$\text{and } K_{\min} = \sigma_{\min} (\pi a)^{1/2} = \left(\frac{\nu_{\min} E}{2(a-x)^{1/2}} \right) (\pi a)^{1/2}$$

[18]

Substitution of equations [17] and [18] into equations of [16] yields

$$da/dN = c \left[\frac{\nu_{\min} E (\pi a)^{1/2}}{2(a-x)^{1/2}} \left(\frac{1}{R} - 1 \right) - 6.4(1-0.85R) \right]^m,$$

R > 0.1 [19]

Letting $da/dN = 1/f * da/dt$, where f is frequency and assuming da/dt is constant, then the crack length may be expressed as $a = da/dt * t$ or $a = (da/dt)^2 * t^2$. Consequently, the crack opening displacement, \min , can be expressed as

$$v_{\min} = \frac{1.128}{E} (da/dt * t)^{-1/2} \left(\frac{R}{1-R} \right) \left[(da/dt)^2 t^2 - x^2 \right]^{1/2}$$

$$* [5.629 * 10^3 * (f * da/dt)^{0.395} + 6.4(1-0.85)]$$

$$R > 0.1 \quad [20]$$

By applying equations [20] to equation [10], the limit of crack growth rate, $(da/dt)_{\text{limit}}$, above which deposit induced closure should not occur, may be calculated.

III. EXPERIMENTAL PROCEDURE

3.1 Specimens

Experiments were performed by 1018 carbon steel plate (2.15 x 1.6 x 0.63 cm) specimen with calcareous deposits on the top side, as shown in Figure 3-1. The specimens were obtained from the experiments Mao conducted (23). The exposure time for each specimen was described previously (23), as shown in Table 3-1. Mao's experimental procedure is briefly described below:

- (1) The specimen (2.15 x 4.90 x 0.63 cm) surface to be exposed was ground and polished with # 600 SiC paper.
- (2) All other areas of the specimen were coated with vinyl spray.
- (3) The electrolyte was sand-filtered, once-through natural sea water, as is available at the Center for Marine Materials Laboratory.
- (4) The experimental variables were set as follows: potential (either -1.00V SCE or -0.85V SCE), water velocity (1 l/min), cyclic frequency (0.1 Hz), water

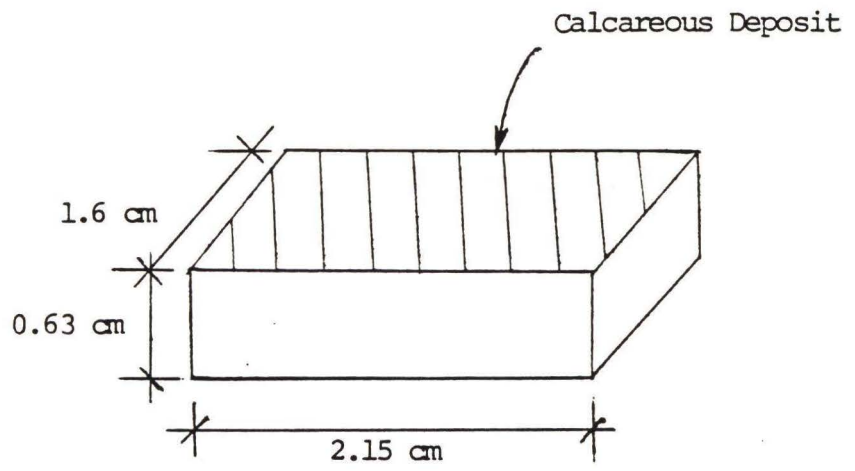


Figure 3-1 Specimen

Specimen	Time (Sec.)
#10	4.68E+4 ----- 13 hours
#29	2.59E+5 ----- 3 days
#16	4.32E+5 ----- 5 days
#06	3.46E+6 ----- 40 days
#18	3.72E+6 ----- 43 days

Table 3-1 Exposure time for different specimens

(-0.85V SCE)

temperature (21 -25° C range), and salinity (approximately 34ppt).

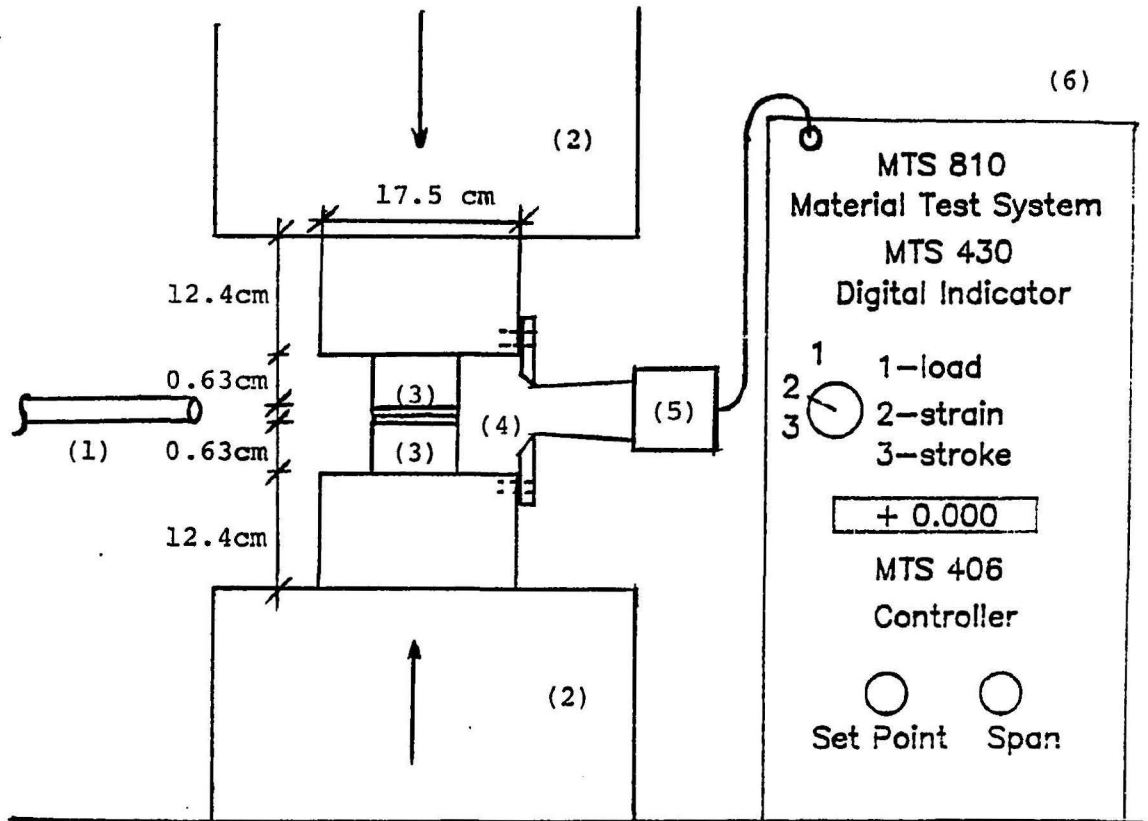
(5) Upon termination of a particular experiment the specimen was removed from the bath, rinsed with alcohol and placed in a desiccator.

3.2 Equipment Description

Tests were performed using a Material Test System, as shown schematically in Figure 3-2. There were two sections in this system (controller and digital indicator). The experiment involved loading calcareous deposits so as to determine the stress-displacement character and degree of compaction. The strain of calcareous deposits was measured in two ways, (1) using an optical microscope and (2) using a clip gage (see Figure 3-2).

3.3 Procedure

(1) Mao's specimen (23) were sectioned into three parts, with dimensions for each as 2.15x 1.6x 0.63 cm. Two of these were loaded, and the third was not. The specimens were surface ground on a plane normal to that of the



- | | |
|---------------------|--------------------------|
| (1) Microscope | (4) Calcareous Deposits |
| (2) Loading Machine | (5) Clip Gage |
| (3) Specimens | (6) Material Test System |

Figure 3-2 Experimental Setup

deposit, so that thickness could be measured at locations away from the edge.

(2) The speed of loading machine was 0.01 cm/min. This was controlled by a turning set-point cursor to permit adequate control of displacements. Periodically, the machine was momentarily stopped to measure the thickness of calcareous deposits and to record the applied stress.

(3) Viewing through a microscope, the thickness of deposits was measured by determining the distance between two lines on the specimens. However, the reading of load and strain for the clip gage was obtained from a digital indicator.

(4) Calcareous deposit thickness was characterized by examination before and after loading in an ISI Super IIIA Scanning Electron Microscope (SEM). Specimen preparation involved viewing edge-on; and the average value of measurements was calculated.

IV. RESULTS AND DISCUSSIONS

4.1 Calcareous Deposit Thickness

Figures 4-1 and 4-2 show the micrographs of calcareous deposits before and after compression for specimens maintained at -0.85V (SCE). Figure 4-3 shows the variation of thickness of calcareous deposits as a function of exposure time before and after compression for specimens maintained at -0.85V (SCE). The reduction percentage is shown in Table 4-1 for the specimens at potential -0.85V (SCE). The average compaction is 25 percent for the specimens at potential -0.85V (SCE) as shown in Figure 4-3. Assuming the same average compaction for the specimens at -1.00V (SCE), the compressed thickness vs. exposure time for specimens polarized to -0.85V (SCE) and -1.00V (SCE) can be formulated, as shown below

$$y = 5.075 \text{ E-6} * \log t - 1.935 \text{ E-5} \quad -0.85\text{V SCE [25]}$$

$$y = 0.744 \text{ E-5} * \log t - 2.497 \text{ E-5} \quad -1.00\text{V SCE [26]}$$

- 37 -
#18 (1510X)



#10 (1560X)

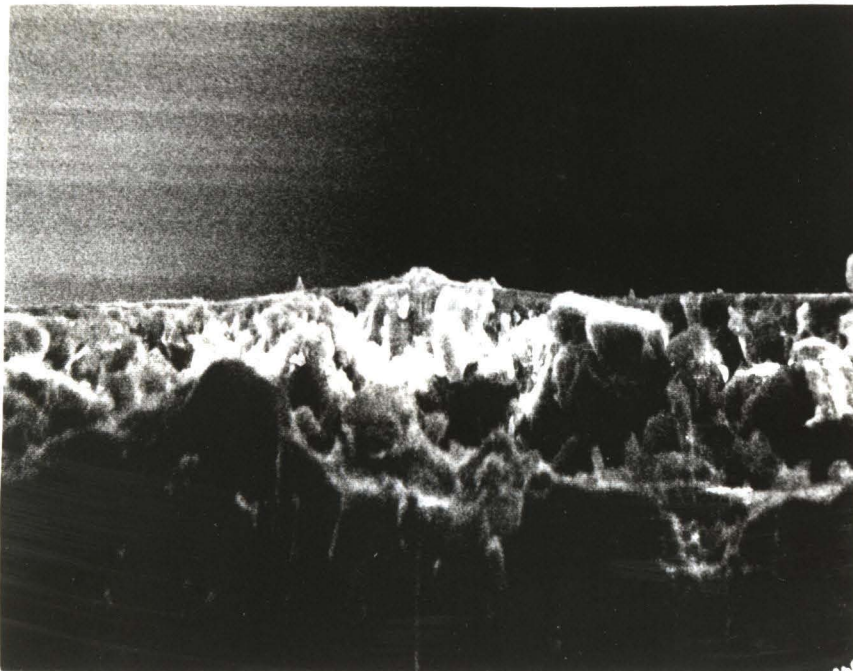
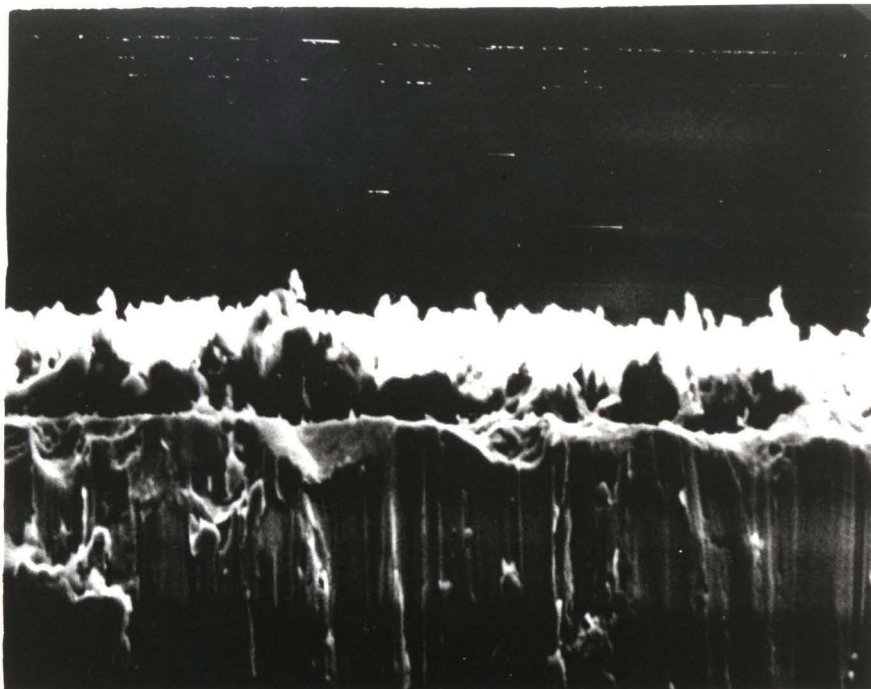


Figure 4-1 Photograph of Calcareous Deposits
After Compression (#13 and #10, -0.85V SCE)

Before (1500X)



After (1500X)

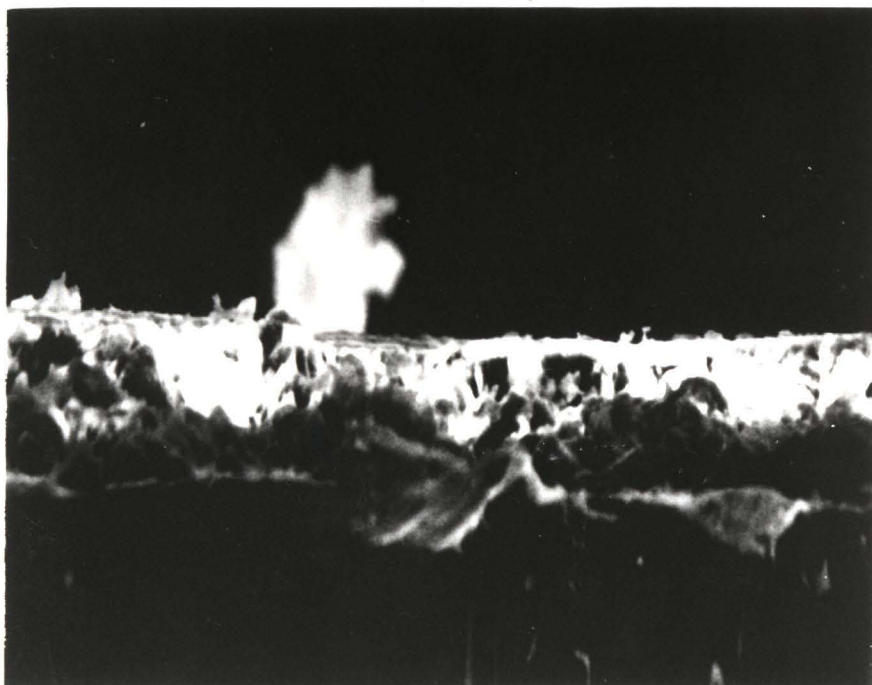


Figure 4-2 Photograph of Calcareous Deposits
Before and After Compression (#06, -0.85V SCE)

Specimens	Time (sec)	Uncompressed Thickness (1.E-5 m)	Compressed Thickness (1.E-5 m)	Reduction Percentage
#10 (-0.85v)	4.68E+4	1.085	1.052	3.04%
#29 (-0.85v)	2.59E+5	1.462	1.057	27.70%
#16 (-0.85v)	4.32E+5	1.273	1.156	9.19%
#06 (-0.85v)	3.46E+6	1.545	1.197	22.52%
#18 (-0.85v)	3.72E+6	3.186	1.098	65.54%
#21 (-1.00v)	5.36E+6	1.650	1.225	25.75%

Table 4-1. Reduction Percentage of Calcareous Deposition Thickness

Before * After o

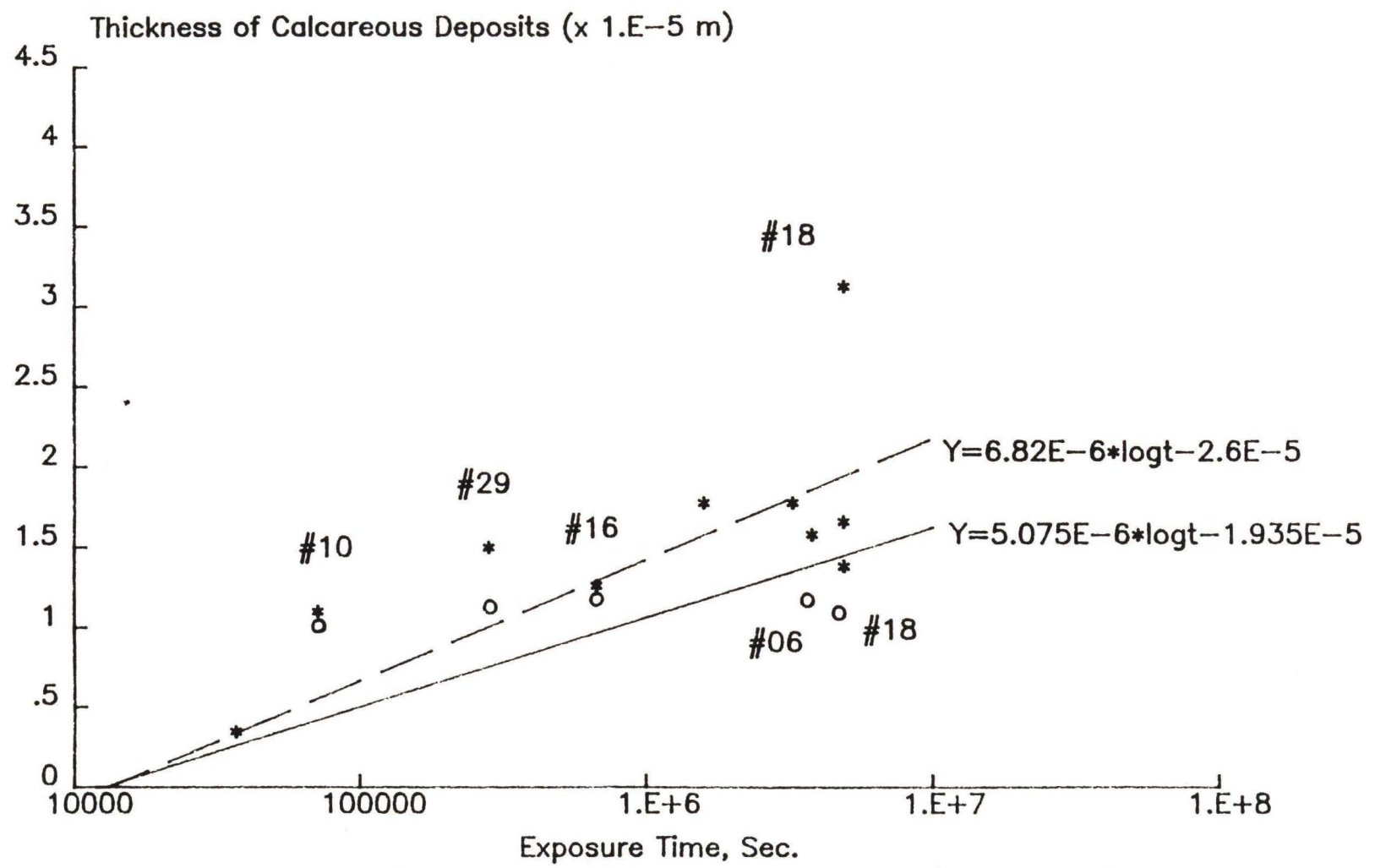


Figure 4-3 Thickness of Deposits vs. exposure time (-0.85V SCE)

Before * After o

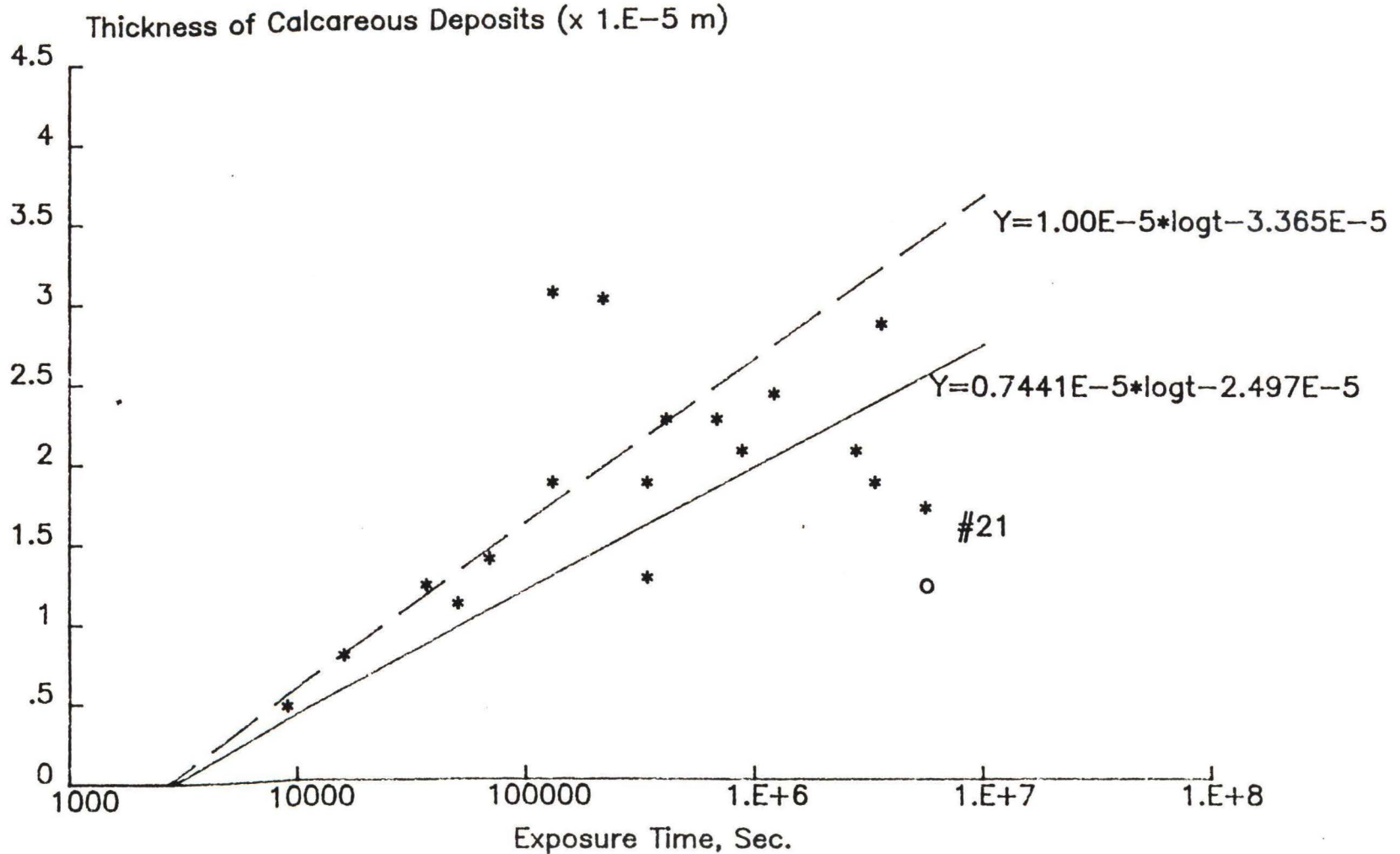


Figure 4-4 Thickness of Deposits vs. exposure time (-1.00V SCE)

The reduction of calcareous deposit thickness ranged from 0.5 E-6 m to 4 E-6 m . For specimen #18, however, there was a large reduction in thickness (21 E-6 m) of calcareous deposits. This may be a consequence of an inherent variability of the phenomenon under investigation which caused specimen #18 to be more porous than other specimens. The fact that seawater temperature was not controlled could also have been a factor.

The fact that thickness of calcareous deposit layers at -1.00V (SCE) was fifteen percent greater than at -0.85V (SCE) presumably resulted from the higher current density at former potential for the post-10000 second period. Consequently, crack closure should be more likely at -1.00V (SCE) than at -0.85V (SCE) . Vosikovsky (25) also discussed the effect of potential on corrosion fatigue crack growth rate. He suggested that cathodic potentials about -1.00V (SCE) increase the intermediate ΔK range FCGR (Fatigue Crack Growth Rate) to values higher than those for free corrosion potentials (-0.70V SCE). There is a possibility that hydrogen embrittlement is the mechanism responsible for the acceleration of crack growth. The more negative potentials increase the thickness of calcareous deposits,

but they also increase the possibility of hydrogen embrittlement.

In addition, the effect of frequency on calcareous deposit growth rate is not clear. Hartt et al (26) have suggested that raising the frequency increases the pumping efficiency; the solution is ejected faster from the crack and is more thoroughly mixed with the bulk solution. However, at low frequency, calcareous deposits may have enough time to precipitate and stick on the metal surface. Consequently, it is hard to state the relationship between frequency and calcareous deposit growth rate.

4.2 Wedging Stress Analysis

The plots of applied load versus the reduction of calcareous deposit thickness are displayed in Figures 4-5 through 4-8. In general two different slopes were observed. The average slope of the lesser one is $6 \text{ E}6 \text{ Kg/m}$, and the steeper one is infinite as measured by the microscope. By using a clip gage the average value of the lesser slope is $5.95 \text{ E}6 \text{ Kg/m}$ and the steeper one is $2.42 \text{ E}7 \text{ Kg/m}$. It is thought that initially the slope is indicative

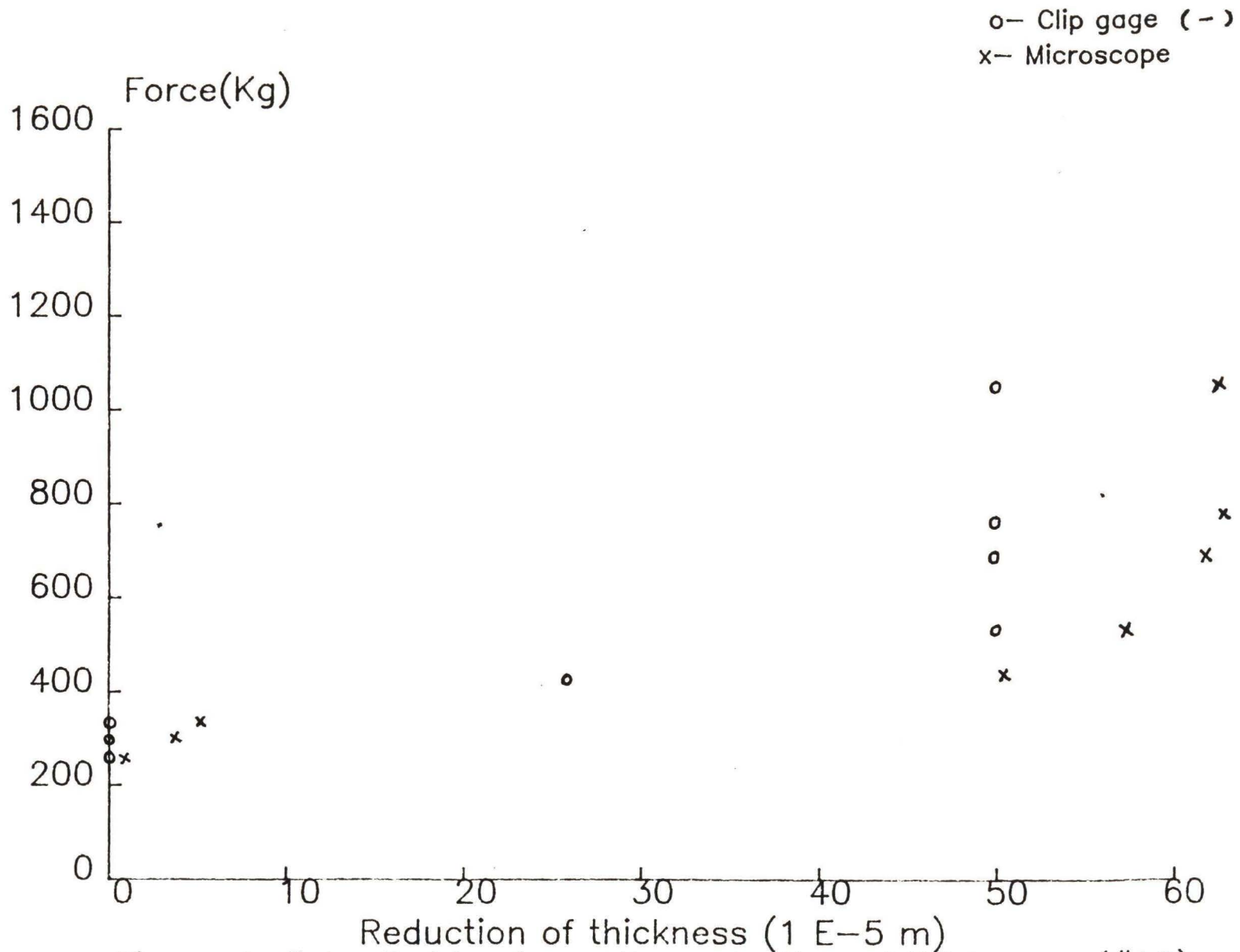


Figure 4-5 Applied loads vs. the reduction of thickness (#10)

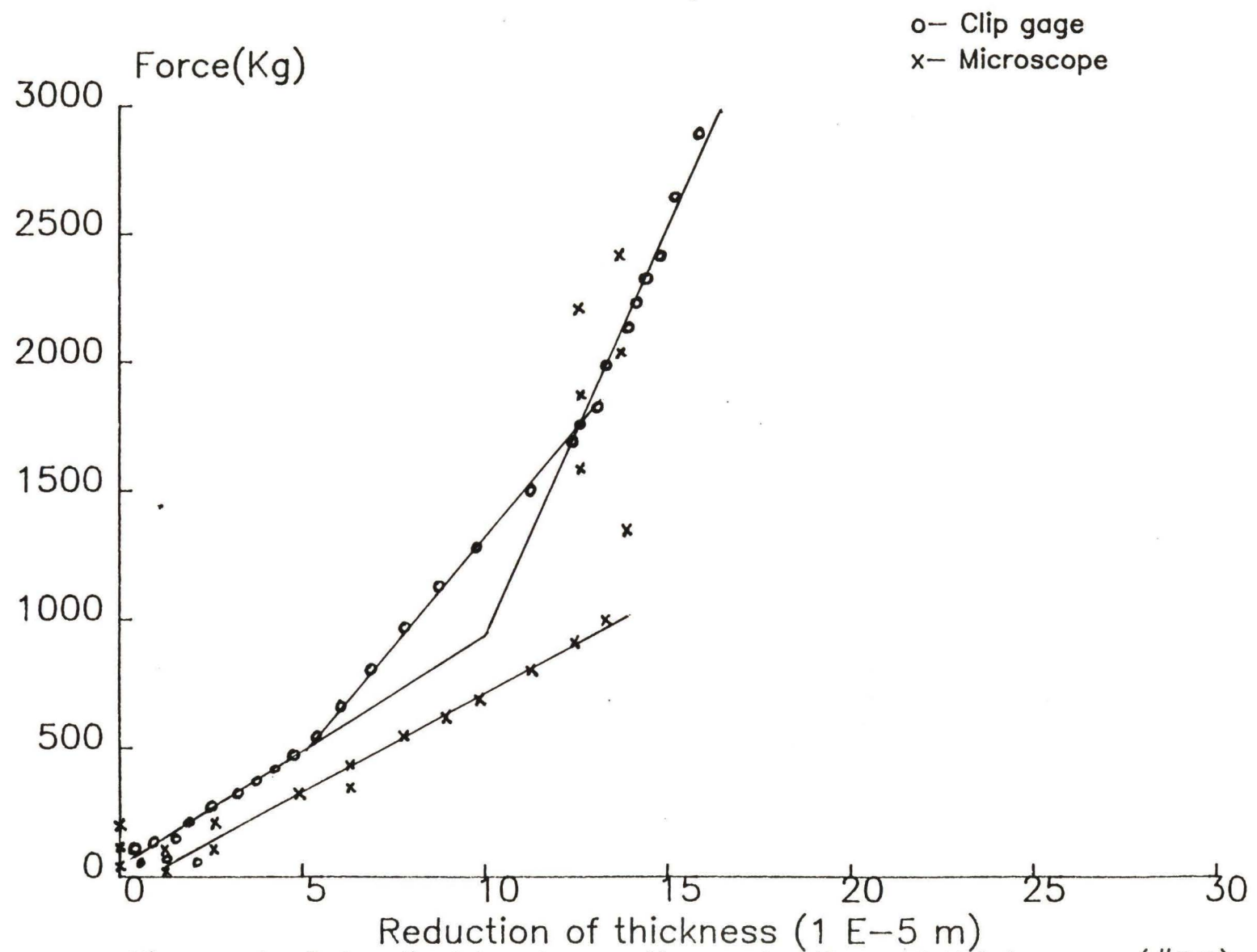


Figure 4-6 Applied loads vs. the reduction of thickness (#29)

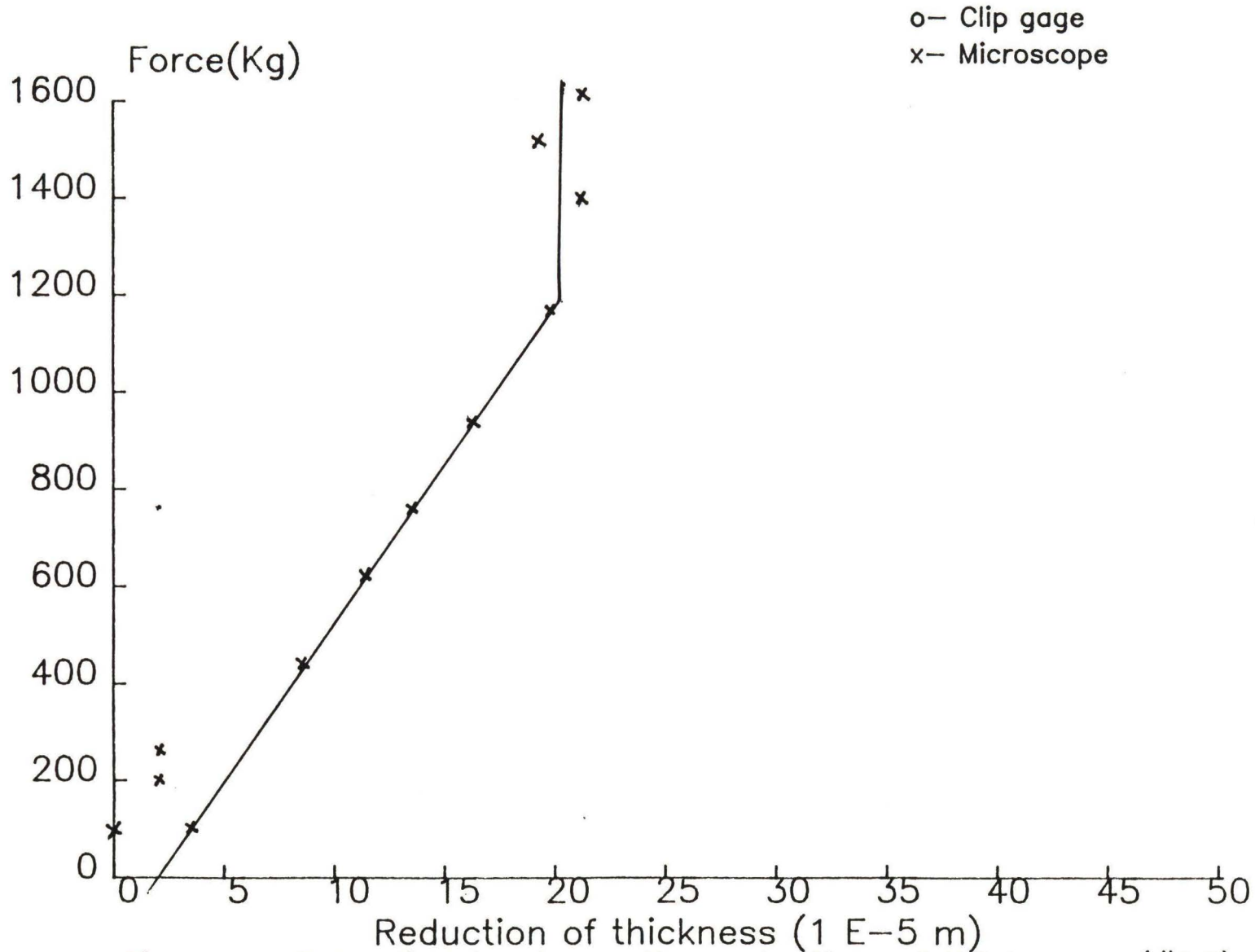


Figure 4-7 Applied loads vs. the reduction of thickness (#06)

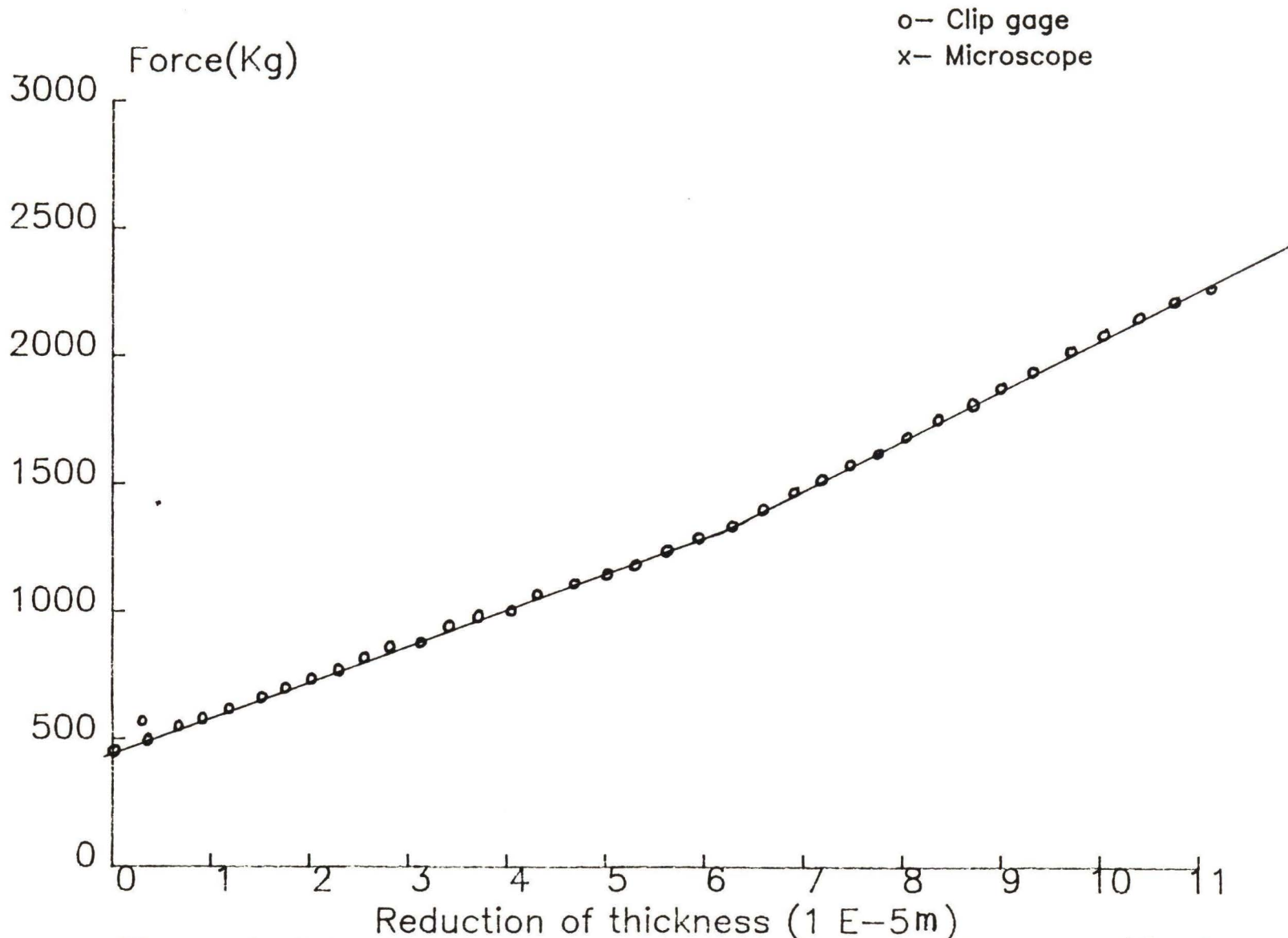


Figure 4-8 Applied loads vs. the reduction of thickness (#18)

of compacting the relatively porous deposits, and the transition to a higher slope reflects completion of this and continued elastic straining of both the deposit and steel.

However, the modulus of the experiment data does not agree with the value of $4.137E4 \text{ MN/m}^2$ for limestone. A possible reason may be rocking of the specimen during compression or nonparallel alignment of test parts. Thus, the calculation of stress based upon contact area becomes uncertain. This may also explain the large displacements for Figure 4-6 through 4-8 compared with Figure 4-3.

The consequence of deposit formed within the crack is that its presence may lead to earlier contact between crack surfaces than if no deposit is present, thereby raising K_{Op} (defined in Figure 1-9) and thus reducing the effective ΔK . The crack will be "wedged closed" (28). For Figures 4-6 through 4-8 the break point for the two slopes may be related to wedging stress intensity. However, the crack length, a , also is an important factor to determining the wedging stress intensity.

4-3 The Limit of Corrosion Fatigue Crack Closure

The limit of corrosion fatigue crack growth rate versus time is shown in Figure 4-9 which is obtained by the application of equations [20] and [10] for two different locations, 0.1Hz, 0.1 load ratio and -0.85V (SCE). From 10,000 to 40,000 seconds (2.78 to 11.11 hours) the limit crack growth rate increases with increasing time. For post-40,000 seconds (11.11 hours) the limit crack growth rate decreases with increasing time. The reason may be that the thickening rate of the calcareous deposit is less than the rate of change of the crack opening displacement for the former case ;whereas, for the latter case the thickening rate of the calcareous deposit could compare with or even exceed the rate of change of the crack opening displacement. In addition, Figure 4-9 also reveals that the present type of closure is most likely at the 0.9a location and least likely at 0.1a. The possible explanation is that the crack opening displacement at the crack tip is less than that away from crack tip. However,

$V = -0.85V$ SCE

$f = 0.1\text{Hz}$, $R = 0.1$

$X = 0.1a$

$X = 0.9a$

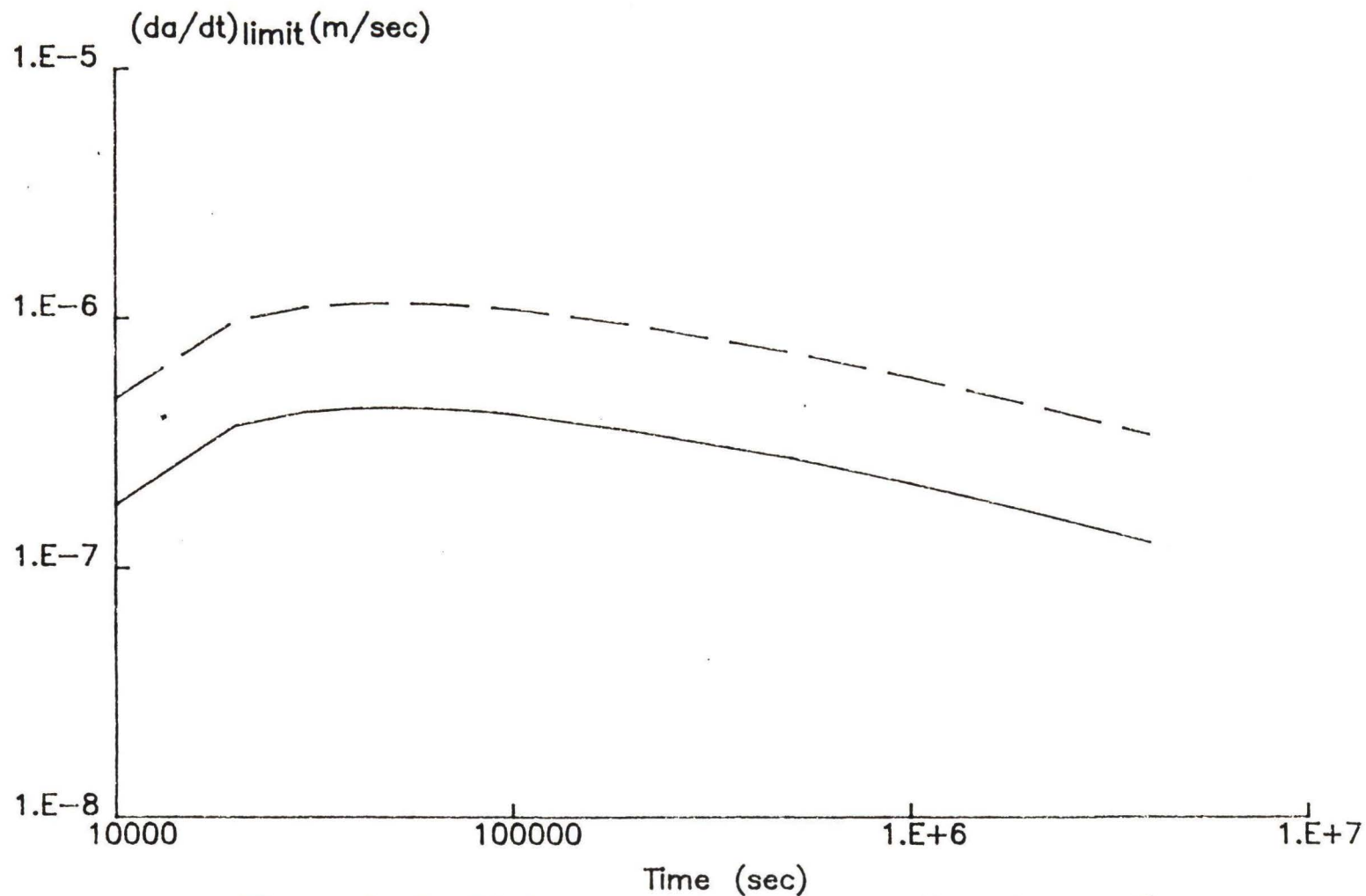


Figure4-9 Plot of limit crack growth rate vs. time

this explanation can be attenuated by the fact that the deposit had less time to growth near the crack tip.

Figure 4-10 shows different trends for the limit crack growth rate, which are a function of load ratio, for two different potential levels, crack positions, and 0.1Hz frequency. The limit crack growth rate, above which deposit induced closure may not occur, is about 1% to 6% lower for this model than that indicated by the work in reference 22. The main reasons for this relatively small difference is that the two terms which have been introduced here (reduction of deposit thickness and a load ratio dependent threshold stress intensity range) have opposite effects on the limit crack growth rate. Therefore the range of limit crack growth rate over which closure has been predicted to occur in this paper is essentially the same as determined previously.

Vosikovsky (13) concluded that the ΔK versus da/dN curves were shifted upward (increased da/dN) as the R value increased. This is similar to the trend of Figure 4-10. This is consistent with the fact that crack closure should be more likely at low load ratio. Figure 4-10 also reveals

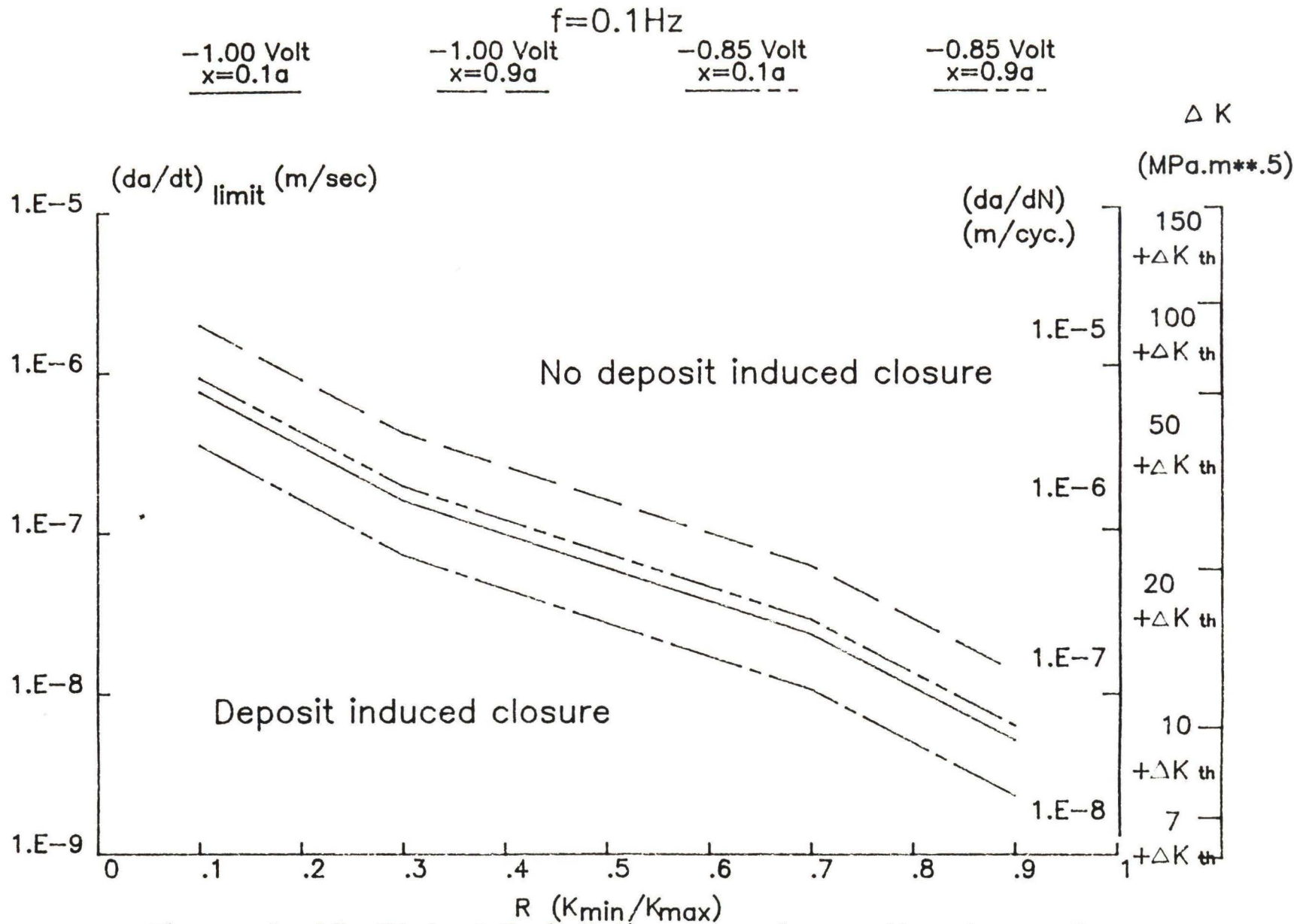


Figure 4-10 Plot of limit fatigue crack growth rate vs. R

that the minimum condition for closure occurs at a lesser crack growth rate for the -0.85V (SCE) case than for -1.00V (SCE). The reason is that the deposit thickness is greater for -1.00V (SCE) than -0.85V (SCE). Consequently, $(da/dt)_{\text{limit}}$ should be shifted to an even higher value in cases of excessive cathodic polarization. Of course, no consideration is given in this argument to the possibility of hydrogen embrittlement.

Equivalent ΔK and $(da/dN)_{\text{limit}}$ values, calculated from Equation [16], are also shown in Figure 4-10, where ΔK_{th} is $6.4(1-0.85*R)$. Thus, calcareous deposit induced closure should be expected at $R=0.9$ and $f=0.1\text{Hz}$ when crack growth rate is less than approximately $0.63\text{E}-08$ m/sec (9.57 Mpa $\sqrt{\text{m}}$) for potential -0.85V (SCE). Also, the further the da/dt (or ΔK) is below this threshold value, the greater the probability and magnitude of such closure.

Figures 4-11 and 4-12 express the limit crack growth rate with variable frequencies in two different ways; the first uses da/dN as a dependent parameter whereas the second uses da/dt . As frequency decreases to 0.01Hz , the limit crack growth rate $(da/dN)_{\text{limit}}$ increases and the

$V = -0.85V(\text{vs. SCE})$

$f=0.01$

$f=0.1$

$f=1.0$

$f=10.0$

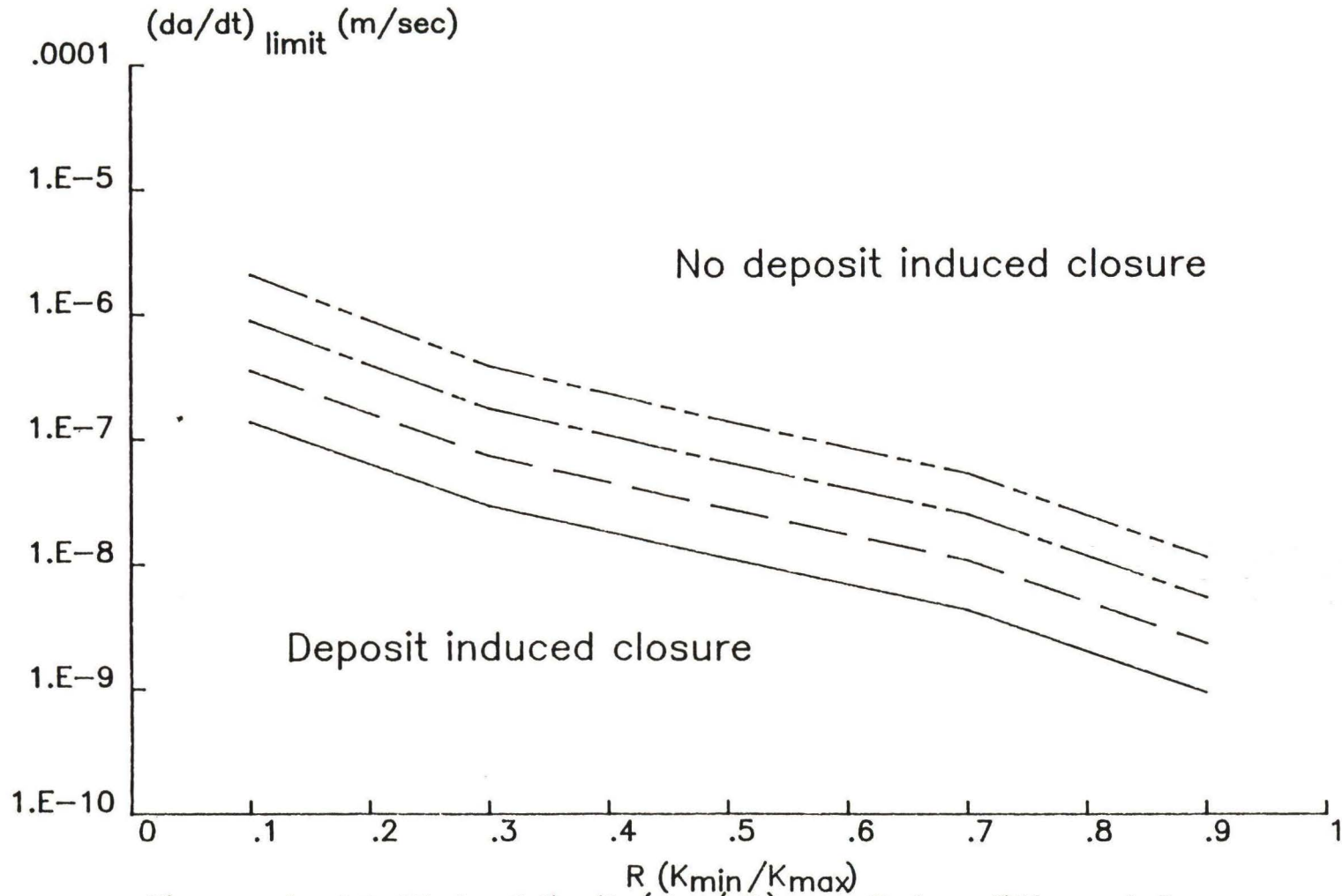


Figure 4-11 Plot of limit (da/dt) vs. R for different frequency

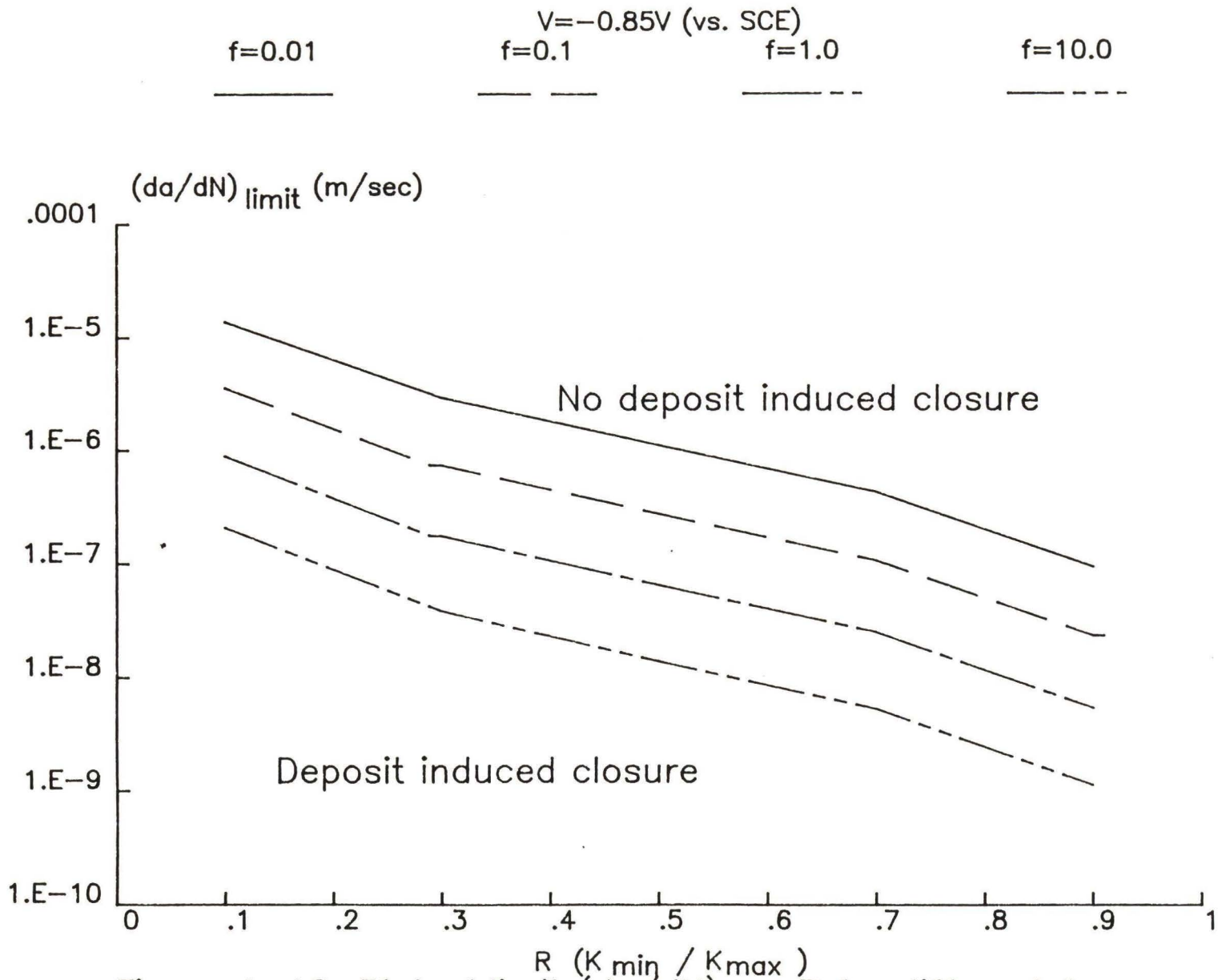


Figure 4-12 Plot of limit (da/dN) vs. R for different frequency

possibility of a crack closure increases. Scott and Silvester (17) found that decreasing the frequency to 0.1 and 0.05 Hz resulted in crack growth rates about four to five times those in air, when ΔK was about 20.0 MPa \sqrt{m} at $R = 0.1$, and in seawater at 20 C. Consequently, the limit crack growth rate $(da/dN)_{\text{limit}}$ for 0.01Hz may shift to lower values which is different from Figure 4-12. The reason for different results may be that the effect of frequency on calcareous deposit growth rate is not clear.

In addition, the limit crack growth rate for closure should be affected by other variables not examined in this thesis, such as temperature, flow velocity of the electrolyte and load wave form. Obviously, complete quantitative characterization of the effects of all these variables is not feasible. Data for fatigue crack growth rate, therefore, must be obtained under conditions simulating the intended service application as closely as possible.

V. CONCLUSIONS

1. Results indicate the porous nature of the deposits and that the potential exists for deposits being compressed under applied load.

2. Wedging stress is caused by precipitated material inside a fatigue crack and it may oppose the applied stress. Thus, ΔK_{eff} is reduced leading to lower crack growth rate.

3. A model has been developed to predict the crack growth rate below which calcareous deposit induced closure occurs. This model predicts the following:

(1) When the thickness of calcareous deposits can not compare with crack opening displacement crack closure should not occur. In contrast closure should occur for the thickness of calcareous deposits greater than the crack opening displacement.

(2) The limit crack growth rate increases, at first, and then, decreases with the exposure time.

(3) Load ratio and cathodic polarization level effect calcareous deposit induced crack closure. Disregarding hydrogen embrittlement, the limit crack growth rate increased as potential was made more negative. For a given frequency crack closure is predicted to be more likely at low load ratio.

BIBLIOGRAPHY

1. Uhlig, H.H., "Corrosion and Corrosion Control", John Wiley & Sons Inc. New York, 1971, p.58.
2. Hartt, W.H., Culberson, C.H., and Smith, S.W., "Calcareous Deposits on Metal Surfaces in Sea Water --- A Critical Review" Corrosion, Vol. 40, 1984, pp. 107-111.
3. Humble, R.A., "Cathodic Protection of Steel in Sea Water with Magnesium Anodes" Corrosion, Vol. 4, 1948, pp. 358-370.
4. Lyashchenko, A.E., Glikman, L.A., and Zobachev, Yu E., "Some Features of Influence of Cathodic Polarization on the Corrosion Fatigue Strength of Steel Samples with a Notch" Soviet Mat. Sci., Vol. 9, 1975, pp. 496-499.
5. Hartt, W.H., and Hooper, W.C., "The Influence of Cathodic Polarization upon Fatigue of Notched Structural Steel in Sea Water" Corrosion, Vol. 34, 1978, pp. 320-326.
6. Martin, P.E., and Hartt, W.H., "Endurance Limit Enhancement of Structural Steel in Sea Water by Cathodic Protection" Proceedings Offshore Technology Conf., April 30- May 3, 1979, Houston, pp. 1331-1340.
7. Hartt, W.H., and Hooper, W.C., " Endurance Limit Enhancement of Notched, 1018 Steel in Sea Water -- Specimen Size and Frequency Effects, " Corrosion, Vol. 36, 1980, pp. 107-111.
8. Velden van der, R. , Ewalds, H. L. , Schultze, , W.A. , and Punter, A., " Anomalous Fatigue Crack Growth Retardation in Steels for Offshore Applications " ASTM, STP 801, 1983, pp. 64-80.
9. Gilbert, P.T. , Metallurgical Reviews, Vol. 1, Part 3, 1956, pp. 379-417.
10. LaQue, F.L. , "Marine Corrosion" John Wiley & Sons Inc. New York , 1975, p. 224.

11. Jaske, C.E., Payer, J.H., and Balint, V.S., "Corrosion Fatigue of Material in Marine Environments", Battelle Memorial Institute, New York, 1981, p. 15.
12. Daris, P.C., "Fatigue -- An Interdisciplinary Approach" Proceedings 10th Sagamore Conf. , Syracuse University Press, Syracuse, N.Y., 1964, p.107.
13. Vosikovsky, O., "Effects of of Stress Ratio on Fatigue Crack Growth Rates in X-70 Pipeline Steel in Air and Saltwater", J. Testing and Eval. 8(2), pp.68-73 (March, 1980).
14. Scott, P. M. et al, "The Effect of Sea Water Corrosion in Fatigue Crack Propagation in Structural Steel", Proceedings of Offshore Steel Conference, Welding Institute, England, November, 1978, pp. 387-414.
15. Rolfe, Stan and Barson John, Fracture and Fatigue Control in Structures--- Application of Fracture Mechanics, p. 224.
16. Vosikovsky, O., "Fatigue-Crack Growth in an X-65 Line-Pipe Steel at Low Cyclic Frequencies in Aqueous Environments", Trans, ASME, J. Eng. Mater. and Technol., Series H, 97 (4), pp. 298-304 (October, 1975).
17. Scott, P. M., and Silvester, D. R. V., "The Influence of Seawater on Fatigue Crack Propagation Rates in Structural Steels", Department of Energy, UK Offshore Steels Research Project, Interim Technical Report UKOSRP 3/03 (December 19, 1975) Barson, J.M., ASTM STP 536, 1976 pp.182.
18. Socie, D.F. and Antolovich, S.D., "Subcritical Crack Growth Characteristics in welded ASTM A 537 Steel", Welding J. 53(6), pp. 267-s-271-s(June, 1974).
19. Elber, W., "Fatigue Crack Closure Under Cyclic Tension" Engineering Fracture Mechanics, Vol. 2, No.1, July 1970, pp. 37-45.
20. Ritchie, R.O. "Some Considerations on Fatigue Crack Closure at Near-Threshold Stress Intensities Due to

- Fracture Surface Morphology" Met. Trans. A, Vol. 13A, 1982, pp. 937-940.
21. Scott, P.M., Silvester, D.R.V., and Thorpe, T.W., "Rate-Determining Process for Corrosion Fatigue Crack Growth in Ferritic Steel in Seawater" Corrosion Science, Vol. 23, No. 6, pp.559-575, 1983.
 22. Hartt, W. H. and Mao, W. "Calcareous Deposit Induced Closure of Fatigue Cracks - An Initial Analysis" Fourth International OMAE Symposium, Feb. 17-21, 1985, Dallas.
 23. Mao, W., Hartt, W.H., and Smith, S.W., "Growth Rate of Calcareous Deposits upon Cathodically Polarized Steel in Sea Water" Corrosion/85, Boston, March 25-29, 1985.
 24. Boresi, A.P., Sidebottom, O.M., Seely, F.B., Smith, J.D., Advanced Mechanics of Materials, P.562, Fourth Edition, 1984.
 25. Scott, P.M., and Silvester, D.R.V., "The Influence of Mean Tensile Stress on Corrosion Fatigue Crack Growth in Structure Steel Immersed in Sea Water," Interim Tech. Report 3/2, Dept. of Energy, U.K. Offshore Steels Research Project, May 25, 1977.
 26. Hartt, W.H., Tennant, J.S., and Hooper, W.C. in Corrosion Fatigue Technology, ASTM STP642, American Society for Testing and Materials, 1978, pp.5-18.
 27. Vosikovsky, O., "Effect of Mechanical and Environmental variables on Fatigue Crack Growth Rates in Steel. A summary of Work Done at Cammet" J. of Canadian Metallurgical Quarterly, Vol. 19. pp.87-97, 1980.
 28. Ritchie, R.O., Suresh, S., and Zamiski, G.F. "Oxide-Induced Crack Closure. An Explanation for Near-Threshold Corrosion Fatigue Crack Growth Behavior" Metallurgical Transactions A, Volume 12A, August 1981, pp.1435-1443.
 29. Jones, B.F. "Fatigue Crack Growth Rates of Steels in Aqueous Environments: The Influence of Environmental, Microstructural and Geometric Factors" Materials

Department, Admiralty Marine Technology Establishment,
Poole, Dorset, UK.

